# Kilometre-Scale Assessment of the Adriatic Dense Water Multi-Decadal Dynamics

**Petra Pranić[1], Cléa Denamiel[2,3], and Ivica Vilibić[2,3]**

[1]Institute of Oceanography and Fisheries, Šetalište I. Meštrovića 63, 21000 Split, Croatia.

[2] Ruđer Bošković Institute, Division for Marine and Environmental Research, Bijenička cesta 54, 10000 Zagreb, Croatia.

[3]Institute for Adriatic Crops and Karst Reclamation, Put Duilova 11, 21000 Split, Croatia.

Corresponding author: Petra Pranić (pranic@izor.hr)

**Key Points:**

- The kilometre-scale dense water generation, spreading and accumulation is quantified in the Adriatic Sea during the 1987–2017 period
- About a third of the dense water is generated within the Kvarner Bay which is deeper and warmer than the well-studied main generation site
- The bottom layer renewal of the accumulation sites is annual in the Kvaner Bay and up to decadal in the deepest Adriatic pits

## Abstract

The North Adriatic Dense Water (NAddW) – the densest Mediterranean water generated by extreme cooling during wintertime hurricane-strength winds – drives the thermohaline circulation, ventilates the deep layers, and changes the biogeochemical properties of the Adriatic Sea. However, modelling the dynamical properties of such dense water at the climate scale has been a challenge for decades due to the complex coastal geomorphology of the Adriatic basin not properly reproduced by existing climate models. To overcome these deficiencies, a 31-year-long simulation (1987-2017) of the Adriatic Sea and Coast (AdriSC) kilometre-scale atmosphere-ocean model is used to analyse the main NAddW dynamical phases (i.e., generation, spreading and accumulation). The study highlights four key results. First, during winter, the NAddW densities are higher in the shallow northern Adriatic shelf than in the deeper Kvarner Bay – where 25-35% of the overall NAddW are found to be generated – due to a median bottom temperature difference of 2°C between the two generation sites. Second, the NAddW mass transported across most of the Adriatic peaks between February and May, except along the western side of the Otranto Strait. Third, for the accumulation sites, the bottom layer of the Kvarner Bay is found to be renewed annually while the renewal occurs every 1–3 years in the Jabuka Pit and every 5–10 years in the deep Southern Adriatic Pit. Fourth, the NAddW cascading and accumulation is more pronounced during basin-wide high-salinity conditions driven by circulation changes in the northern Ionian Sea.



## Plain Language Summary

The densest water in the Mediterranean Sea known as the North Adriatic Dense Water (NAddW) forms during severe winter wind events in the northern Adriatic. This phenomenon which brings oxygen-rich waters to the sea bottom, plays a vital role in sustaining life in the Adriatic Sea. However, due to the complex geography of the Adriatic, accurate representation of NAddW is very challenging and requires fine-resolution atmosphere-ocean models such as the Adriatic Sea and Coast (AdriSC) model. Here, the AdriSC historical simulation is used to study NAddW generation, spreading and accumulation. The findings reveal that about a third of NAddW is produced in the Kvarner Bay which is a deeper and warmer than the Northern Adriatic shelf. Further, it is found that NAddW spreads over most of the Adriatic between February and May bringing dense waters to the bottom of the accumulation sites, which are renewed annually in the northern Adriatic, up to every 3 years in the middle Adriatic pit, and up to every decade in the Southern Adriatic Pit. Lastly, the study highlights that NAddW spreading and accumulation are significantly enhanced during periods of higher salinity across the Adriatic, a phenomenon driven by water exchanges with the Ionian Sea.

## 1 Introduction

The Adriatic Sea is a semi-enclosed basin located in the northernmost part of the central Mediterranean Sea (Fig.1). Its diverse and complex geomorphological characteristics (i.e. orography, bathymetry and coastline) influence a wide variety of atmospheric and oceanic processes ranging from long-term dynamics on larger spatial scales (e.g. thermohaline circulation) to short-term phenomena on smaller spatial scales (e.g. extreme wind events, dense water generation, river plume dynamics). One of the main processes driving the Adriatic thermohaline circulation is the formation of North Adriatic Dense Water (NAddW; Zore-Armanda, 1963) that occurs, in winter, over the northern Adriatic shelf and the Kvarner Bay during extreme bora events – i.e., downslope winds strongly influenced by the complex north-eastern Adriatic coastal orography and associated with hurricane-strength gusts up to 50 m $s^{-1}$ (Belušić and Klaić, 2004). In the last 40 years, the Adriatic dense water dynamics has mostly been derived from observations (Artegiani and Salusti, 1987; Gačić et al., 2002; Vilibić and Mihanović, 2013; Querin et al., 2016; Foglini et al., 2016; Paladini de Mendoza et al., 2022) and has been summarized in the review study of Vilibić et al. (2023) as follows. First, the NAddW formation is known to be preconditioned by three main factors: the bora-induced surface heat losses, the northern Adriatic river fresh water influxes, and the advection of more saline water masses from the Ionian Sea. Second, the generated dense water is known to spread towards the Strait of Otranto along the western Adriatic coast at the sea bottom beneath the Po River plume and the Western Adriatic Current. Then, along this path, dense water is known to be partly collected within the ~280-m-deep Jabuka Pit and cascading, mostly through the Bari Canyon, into the ~1230-m-deep Southern Adriatic Pit (SAP). Finally, jointly with the Adriatic Deep Water (AdDW) generated in the SAP through open ocean convection, the remaining part of the NAddW leaves the Adriatic basin through the Strait of Otranto towards the northern Ionian Sea. Additionally, both NAddW and AdDW have been documented to strongly influence the Adriatic–Ionian thermohaline circulation and regime changes as well as the biogeochemistry of the Adriatic Sea (Boldrin et al., 2009; Bensi et al., 2013; Gačić et al., 2010; Batistić et al., 2014; Jasprica et al., 2022).

In terms of numerical modelling, till recently, three different types of approaches have been used to study the Adriatic dense water dynamics. First, short-term simulations (up to 1-2 weeks) have been performed with fine-resolution ocean models using different types of atmospheric forcing (e.g., Dorman et al., 2007; Ličer et al., 2016). Then, longer simulations (up to 8 years) were implemented with the aim to investigate the interannual variability of the Adriatic dense waters (e.g., Mantziafou and Lascaratos, 2008; Oddo and Guarnieri, 2011; Mihanović et al., 2018). Compared to the short-term simulations, they used either much coarser (horizontal and vertical) resolutions in the ocean and/or much coarser atmospheric forcing such as the ERA40 or ERA5 reanalyses from the European Centre for Middle-range Weather Forecast (ECMWF). Some of these simulations also imposed an inappropriate freshwater climatology in the northern Adriatic basin. Finally, the multi-decadal NAddW dynamics has also been investigated with the Mediterranean Coordinated Regional Downscaling Experiment Regional Climate Models (Med-CORDEX RCMs; Ruti et al., 2016) for the 1980–2012 period (Dunić et al., 2019). However, due to their insufficient horizontal resolution in both the ocean (order of 10 km) and the atmosphere (order of 25 to 50 km), these RCMs were not capable of properly reproducing dense water formation in the northern Adriatic shelf which resulted in a noticeable ocean temperature overestimation within the NAddW accumulations sites (Jabuka Pit and SAP).

The kilometre-scale atmosphere-ocean Adriatic Sea and Coast (AdriSC) climate model has thus been recently implemented by Denamiel et al. (2019) with the aim to provide a better representation of the Adriatic dynamics and quantify the impacts of climate change. First, the added value of the kilometre-scale approach has been tested with short-term simulations demonstrating that the AdriSC climate model was better suited to represent the complex Adriatic atmosphere-ocean dynamics during extreme events than coarser models (Denamiel et al., 2020a, b, 2021a). Then, two 31-year-long simulations were performed with the AdriSC climate model: one during the historical period (1987-2017) and one during the future period (2070-2100) for a Representative Concentration Pathways (RCP) 8.5 scenario. Finally, the historical AdriSC simulation was successfully evaluated against in situ and remote-sensing products in both atmosphere (Denamiel et al., 2021b) and ocean (Pranić et al., 2021). Compared to the state-of-the-art Mediterranean and Adriatic models, the AdriSC climate model was demonstrated to not only reduce atmosphere-ocean biases but also to better reproduce the Adriatic Sea dynamics, including the quasi-decadal salinity and current oscillations (Denamiel et al., 2022) driven by the Adriatic-Ionian Bimodal Oscillating System (BiOS; Gačić et al., 2010; Civitarese et al., 2023), the NAddW dynamics in 2015 (Pranić et al., 2023) and the 31-year atmosphere-ocean trends and variability (Tojčić et al., 2023).

Following the studies demonstrating the skills of the AdriSC climate model, the aim of this research is to investigate, for the first time, the multi-decadal Adriatic dense water dynamics during the 1987-2017 period, based on climatological analyses of the AdriSC dense water results at 1-km horizontal resolution. The article is structured as follows. The AdriSC model and the methods used for the climatology analyses are described in Section 2 while the results for the generation, spreading and accumulation of the dense waters are presented in Section 3. The main findings of the study are further discussed in Section 4.

## 2 Model and Methods

### 2.1 Adriatic Sea and Coast (AdriSC) model

The kilometre-scale atmosphere-ocean Adriatic Sea and Coast (AdriSC; Denamiel et al., 2019) climate model is based on the Coupled Ocean–Atmosphere–Wave–Sediment Transport (COAWST) modelling system (Warner et al., 2010). It consists of the Weather Research and Forecasting (WRF; Skamarock et al., 2005) atmospheric model used with two nested grids at 15 and 3 km of horizontal resolution, respectively, one-way coupled with the Regional Ocean Modelling System (ROMS; Shchepetkin and McWilliams, 2009) ocean model, also used with two nested grids at 3 km and 1 km resolution, respectively. Both models use terrain following coordinates in the vertical with 58 levels refined near the land in WRF (Laprise, 1992) and 35 levels refined near the surface and bottom of the ocean in ROMS. More detailed descriptions of the AdriSC model, as well as the evaluation of the AdriSC climate simulation against observations, can be found in Denamiel et al. (2019, 2021b) and Pranić et al. (2021).

Importantly for the Adriatic dense water dynamics, Denamiel et al. (2022) demonstrated that the AdriSC salinity and ocean current speed signals can be explained (except in the deepest part of the SAP) by the BiOS-driven Adriatic phases – up to 61% and 9% (respectively) in the intermediate layer and up to 37% and 31% (respectively) at the bottom. These phases approximately present a 2-year lag compared to the BiOS signal in the Ionian Sea and are anticyclonic for the 1990–1999 and 2007–2011 periods and cyclonic for the 1987-1989, 2000–

2006 and 2012–2017 periods. Denamiel et al. (2022) also pointed out that, due to the influence of extraordinary Eastern Mediterranean Transient (EMT; Roether et al., 2007) conditions in the 1990s, the strongest anticyclonic BiOS-driven phase in the AdriSC model occurred during the 1990-1999 period. Further, Tojčić et al. (2023) analysed the AdriSC atmosphere-ocean trends and variability for the 1987-2017 period and found positive salinity trends over the entire Adriatic Sea – particularly strong in the intermediate layer over the Jabuka Pit and at the bottom of the dense water generation sites – associated with a shallowing of the advection of the saline Levantine Intermediate Water inflow into the Adriatic, a decrease of the AdDW outflow, and a shrinking plus weakening of the Southern Adriatic Gyre at the centre of the SAP.

In this study, the daily bottom potential density anomalies (PDAs) are calculated with the daily bottom temperature and salinity extracted from the 1-km ocean results of the 31-year AdriSC historical simulation (1987-2017), and the function available within the NCAR Command Language (NCL) library (Levitus et al., 1994a, 1994b; Dukowicz, 2000; https://www.ncl.ucar.edu/). Further, throughout the analyses, dense water is considered, in the Adriatic Sea, for PDAs equal to or larger than 29.2 kg $m^{-3}$ based on previous NAddW research (e.g., Mantziafou and Lascaratos, 2008; Janeković et al., 2014; Vilibić et al., 2018).

### 2.2. Climatological analysis

The climatological analyses are performed for the three main dynamical phases of the dense water dynamics: generation, spreading and accumulation. The analyses of the dense water generation are carried out for the two generation sites – northern Adriatic (NA) and Kvarner Bay (KB; Fig. 1). The results are presented in the form of daily time series of subdomain averaged bottom PDA, temperature and salinity for the whole time period of the simulation. The maximum bottom PDAs are calculated for each point of the subdomains in January, February and March (JFM). Also, the day of the year (DOY) in which the maximum PDA value occurred is considered. The results are presented as: 1) probability density functions (PDFs) derived with a kernel-smoothing method for the maximum bottom PDAs as well as bottom temperature and salinity during the DOYs of maximum PDAs, and 2) box plots of yearly maximum PDA and associated DOY, as well as bottom temperature and salinity during these DOYs (in Supplemental Material). A kernel-smoothing method (Bowman and Azzalini, 1997) is used to calculates the probability density estimate based on a normal kernel function and is evaluated for 100 equally spaced points.

Concerning the spreading phase, the analyses are performed for nine transects (T1, T2, T3, T4, T5a, T5b, T6, T7, T8) which are defined along the known dense water pathways. The outward dense water flow rates are calculated only for the bottom layer and are obtained by multiplying the bottom velocities normal to the transect by the bottom PDAs along each transect. The results are shown as monthly time series of cumulative dense water mass transported outward through the transects – i.e., monthly sum of the outward dense water flow rates. The obtained quantity is defined as positive in the northwest direction for all transects except T2, for which it is positive in the northeast direction. Additionally, the climatology of the monthly bottom dense water mass transported outward is also presented as bar plots for all transects.

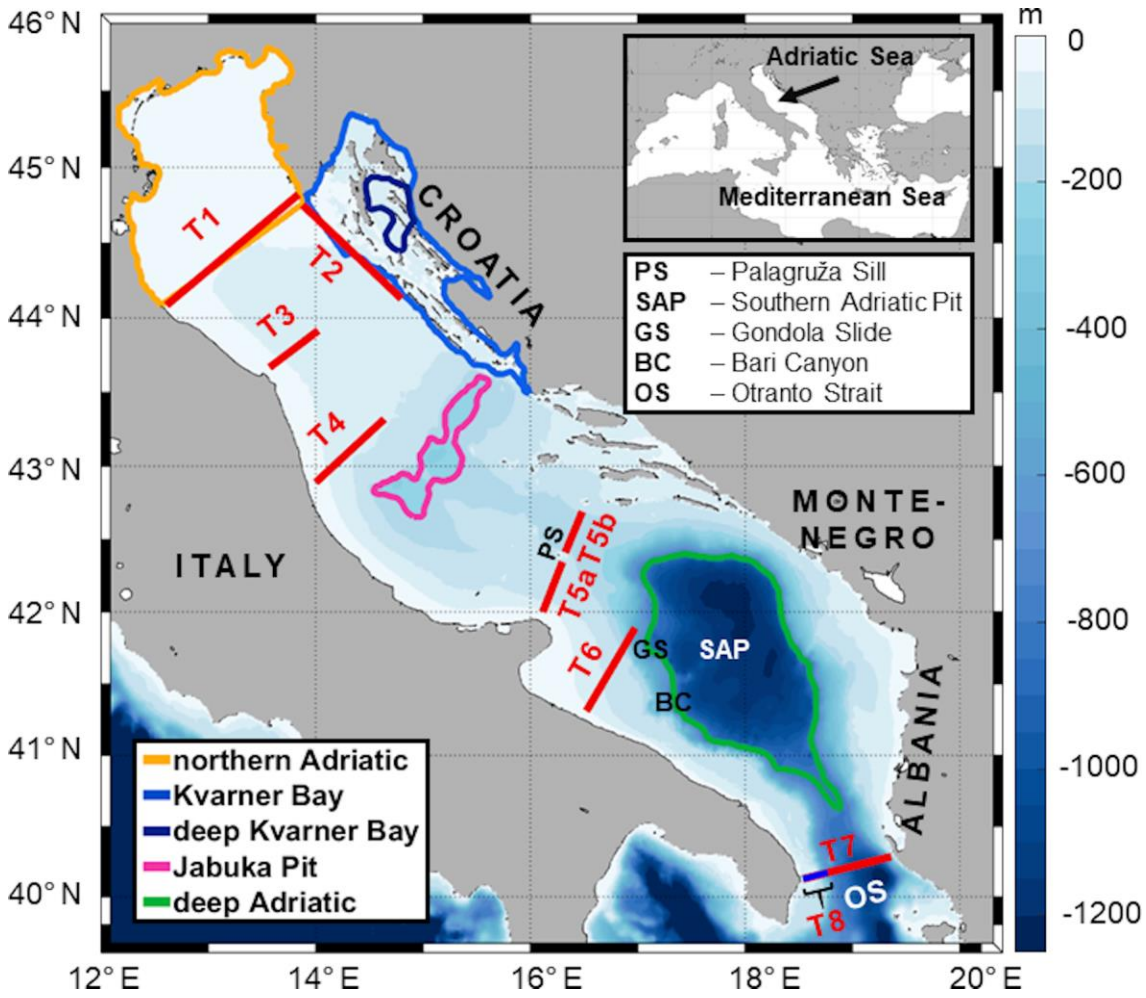


**Figure 1.** Bathymetry of the AdriSC 1-km model domain with indicated geographical terms, as well as the subdomains and transects (red lines) used to study the Adriatic dense water multi-decadal dynamical properties during the 1987-2017 period.

To quantify the dense water accumulation for the whole simulation period, several analyses were conducted for three accumulation sites (subdomains) – deep Kvarner Bay (DKB) with depths above 80 m, Jabuka Pit (JP) with depths above 200 m and deep Adriatic (DA) with depths above 1000 m encompassing the SAP (Fig. 1). The JP and the SAP are well-known and well-researched dense water accumulation sites (e.g., Zore-Armanda, 1963; Querin et al., 2016), while dense waters generated in the Kvarner Bay are gravitationally attracted in DKB which is much deeper than the adjacent open northern Adriatic shelf. Firstly, an mp4 animation of the spatial daily results of the bottom PDA over the Adriatic Sea and the time series of subdomain-averaged bottom PDAs (Movie S1) as well as the time series of subdomain-averaged bottom temperature and salinity are analysed. Then, the maximum bottom PDA and associated DOY as well as the bottom temperature and salinity during these DOYs (in Supplemental Material) are presented as box plots. Lastly, the monthly-averaged bottom PDAs as well as bottom temperature and salinity (in Supplemental Material) are presented as box plots (without outliers).

## 3 Results

### 3.1 Dense water generation

The process of dense water generation is investigated first by analysing the daily time series of averaged bottom PDA, temperature and salinity for the NA and KB subdomains (Fig. 2). The seasonal variability of all three variables in NA is larger compared to KB. In particular, bottom PDAs in NA vary between 27.0 and 30.0 kg $m^{-3}$, while in KB they range from 27.7 to 29.9 kg $m^{-3}$ (Fig. 2a). Also, PDA maximums are often smaller in KB than in NA (by 0.1–0.4 kg $m^{-3}$). The time series of PDA in NA reveals a sharp increase during winter reaching a peak in February, followed by a sharp decrease until the end of summer when the PDA minimums are produced. In KB, a smaller secondary peak in PDA is present during summer, associated with dense water accumulation in the deepest KB sections. In autumn, the larger PDA simulated in KB compared to NA indicates delayed mixing of the entire water column due to the greater depths within KB. Dense waters with PDA equal to or larger than 29.2 kg $m^{-3}$ are generated throughout most of the years, except for 2014 in NA and 1990, 1994–1997, 2007 and 2014 in KB. The years with the strongest dense water generation (indicated by a PDA maximum larger than 29.5 kg $m^{-3}$) are 1989, 1991, 1999, 2000, 2002–2006, 2008, 2012, 2013 and 2017 in NA, and 1987, 1989, 1993, 1999, 2000, 2002, 2004–2006, 2008, 2012, 2013 and 2017 in KB.

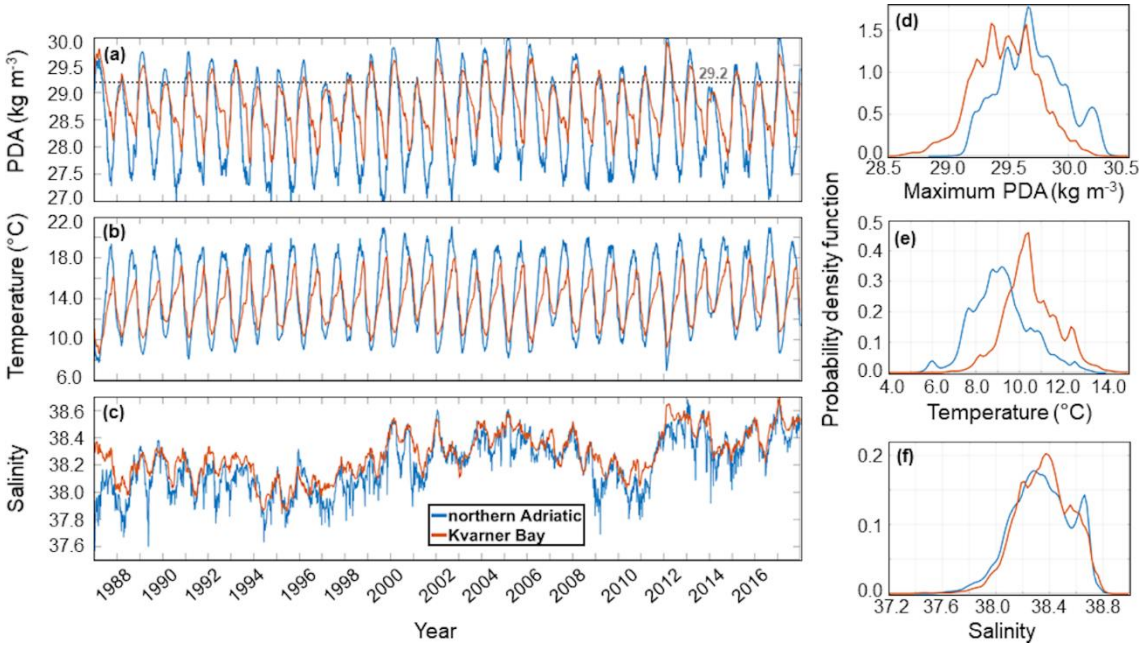


**Figure 2.** Daily time series of bottom (a) PDA, (b) temperature and (c) salinity for the northern Adriatic and Kvarner Bay subdomains during the 1987–2017 period. Probability density functions of (d) maximum bottom PDA, as well as bottom (e) temperature and (f) salinity for the DOY with maximum PDA in the northern Adriatic and Kvarner Bay subdomains during the JFM seasons of the 1987–2017 period.

Bottom temperature varies between 6.5 and 21.0 °C in NA and between 8.0 and 17.0 °C in KB (Fig. 2b). Temperature peaks are mostly reached in late autumn in KB, while in NA they occur in summer, reacting faster to changes in surface heat flux due to its shallower depth. The lowest temperatures were produced during the extreme winter of 2012 in both subdomains. Bottom salinity values are overall larger in KB than in NA (Fig. 2c). In the 1987–1999 period,

salinity varies between 37.6 and 38.4 in NA and between 38.0 and 38.4 in KB. Larger salinities are simulated in the 2000–2008 period in both subdomains, followed by a decrease until 2011. Then, a steep increase occurred leading to large salinities in the 2012–2013 period. Notably, in 2012, salinity in KB reached a peak larger than in NA (by more than 0.1), while the temperature was higher by approximately 2.5 °C. Consequently, very close extreme values of PDA were simulated in the two generations sites. Similarly, in 1987, substantially larger salinity in KB resulted in larger PDAs compared to NA. However, even though 1987 has been documented to have strong dense water formation events (Vilibić and Orlić, 2001), these AdriSC results should be considered with caution due to possible influence of the initial conditions imposed only 2 months before January 1987 during the short spin-up period. Further, a slight salinity decrease occurred after 2013 in both subdomains, followed by an average increase and peaking at 38.7 in 2017. Finally, for both generation sites, positive trends (Tojčić et al., 2023) and influence of the quasi-decadal BiOS-driven phases (Denamiel et al., 2022) are noticeable in the AdriSC bottom salinity time series.

In order to examine the differences in the behaviour of thermohaline parameters between the two generation sites, the PDFs of maximum bottom PDA, as well as bottom temperature and salinity for the DOY with maximum PDA during the winter (JFM) seasons of the 1987–2017 period, are also presented in Fig. 2. Maximum PDAs are generally larger in NA where the highest probabilities are obtained for the PDAs around 29.7 kg $m^{-3}$, while in KB the most probable PDAs range between 29.3 and 29.6 kg $m^{-3}$ (Fig. 2d). Temperatures are generally higher in KB, with the highest probabilities for values around 10–11 °C, whereas in NA, around 9 °C (Fig. 2e). Conversely, the salinity PDFs are very similar in both subdomains, with salinities mostly distributed between 37.8 and 38.8 (Fig. 2f). Slightly higher probabilities are found for salinities around 38.4 in KB and below 38.3 in NA. Hence, dense water generated in NA is denser compared to KB mainly due to its lower temperatures, while the salinity difference between the two formation sites remains small. It should be noticed that despite the maximum heat losses occurring over KB during the dense water generation (e.g., Dorman et al., 2007; Janeković et al., 2014; Denamiel et al., 2021a), the lowest bottom temperatures are found in NA which is 3 times shallower than the deepest part of the KB.

The annual climatology of maximum bottom PDA and associated DOY of maximum PDA during the JFM season between 1987 and 2017 is presented in the form of box plots for both subdomains (Fig. 3 and 4). In NA, the years with the smallest maximum PDAs (median of maximum PDAs < 29.5 kg $m^{-3}$) and therefore the weakest dense water generation are: 1988, 1997, 1998, 2001, 2007, 2009 and 2014 (Fig. 3a). The years with the strongest dense water generation (median of maximum PDAs > 30.0 kg $m^{-3}$) are: 2002, 2005, 2012 and 2017. The remaining majority of the years belongs to the moderate category with maximum PDAs between 29.5 and 30.0 kg $m^{-3}$. In KB, distributions of maximum PDAs are generally smaller than those in NA (Fig. 3b). Median maximum PDAs larger than 30.0 kg $m^{-3}$ are produced only in February–March 2012, which is confirmed by sparse observations in that area indicating a maximum PDA of around 30.0 kg $m^{-3}$ (Mihanović et al., 2013; Raicich et al., 2013). In one half of the remaining years, PDAs range between 29.5 and 30.0 kg $m^{-3}$, while in the other half, they are smaller than 29.5 kg $m^{-3}$.

The median of the DOY of maximum PDA in NA varies between 25 and 70, revealing the interannual differences in the timing of the dense water generation. For example, in 2002, the

major dense water generation event occurred in January without further increases in PDA afterward. Conversely, in 2011, the highest PDA is produced in March, indicating substantial late-winter cooling. Further, some years have a wide range in the distributions of the DOY of the maximum PDA, suggesting the occurrence of either several presumably weak dense water events in different parts of NA or a slow transport of dense water in the bottom layers of the northern Adriatic shelf (Vilibić et al., 2008). The box plots of the DOY in KB are similar to those for NA but with a slight prevalence of the later part of the JFM period. Also, years with wider range in distributions of the DOY are present in KB which indicates the existence of several cooling events.

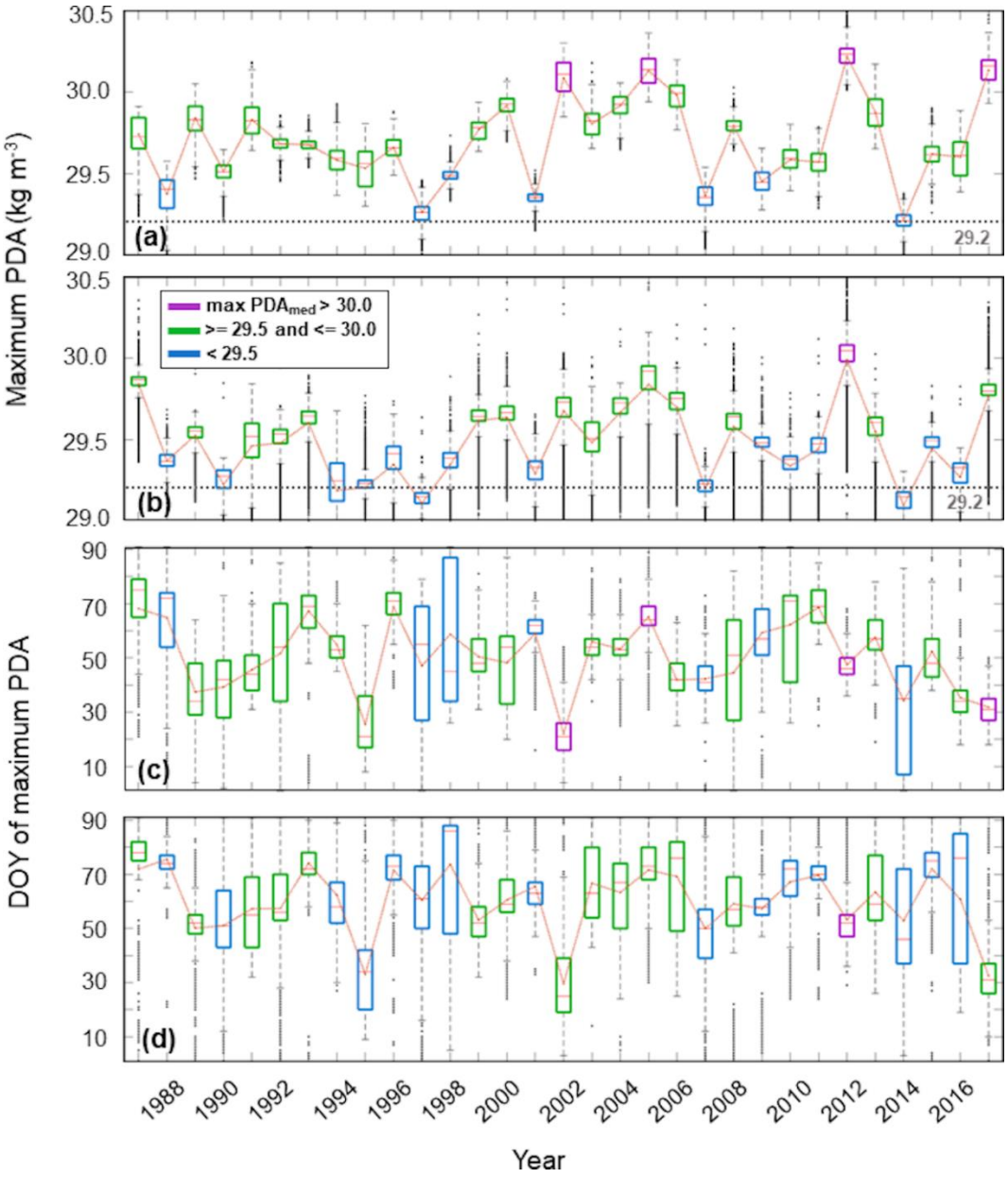


**Figure 3.** Box plots of maximum bottom PDA and DOY of maximum PDA for the (a, c) northern Adriatic (NA) and (b, d) Kvarner Bay (KB) subdomains in the 1987–2017 period. The

red line inside each box plot denotes the median of the distribution. The orange dotted line connects the mean values of the distributions.

### 3.2. Dense water spreading

The spreading of dense water is analysed along different transects across the Adriatic Sea (Fig. 1). First, the time series of monthly bottom dense water mass transported outward through the nine transects are presented in Fig. 4. At T1, located on the southern edge of the northern Adriatic, indicating the dense water outflow solely from the northern Adriatic, the transported dense water mass mostly varies around $-10.0 \cdot 10^{11}$ kg, slightly surpassing this value in 2003 and 2017. The largest mass of dense water is transported through T1 in February 2012, sharply peaking at $-20.0 \cdot 10^{11}$ kg. The amounts of transported dense water mass through T2, marking the boundary between the open sea and the northern half of the Kvarner Bay and indicating dense water mass outflow from the Kvarner Bay only, mostly vary around $-5.0 \cdot 10^{11}$ kg and exceptionally to $-6.8 \cdot 10^{11}$ kg in February 2012. A comparison between T2 and T1 bottom dense water mass outflow, suggests that the outflow from the Kvarner Bay is 2–3 times lower than the outflow from the northern Adriatic, attributing 25–35% of the total generated dense waters to the Kvarner Bay. This estimate is smaller than the previously quantified contribution of the Kvarner Bay to the total dense water formation during winter 2012 found to be around 40% by Janeković et al. (2014). This might be linked to differences in methodology (mass vs. volume transports) but also to the fact that 2012 was an exceptional year for dense water generation with a very dry preconditioning resulting in higher than usual salinities and, hence, PDAs in the coastal Kvarner Bay (Mihanović et al., 2013).

Further southeast, at T3 in the middle Adriatic, the bottom dense water mass varies around $-1.0 \cdot 10^{11}$ kg, while larger values around $-2.0 \cdot 10^{11}$ kg are obtained in 2003, 2006 and 2012. The decrease possibly reflects enhanced mixing between dense waters and ambient waters known to occur in this region (Vilibić and Mihanović, 2013) and strongly modify the dense water outflow. The T4 transect, located north of the Jabuka Pit in the middle Adriatic, shows mostly smaller amounts of transported dense water mass except in 1988, 2000 and 2012 (near $-2.0 \cdot 10^{11}$ kg or larger).

Significant differences are evident between the two transects, T5a and T5b, located in the Palagruža Sill and divided by the island of Palagruža. Until the mid-1990s, the monthly transported dense water mass is much larger at T5b (reaching $-6.0 \cdot 10^{11}$ kg) than at T5a (reaching $-2.0 \cdot 10^{11}$ kg), after which there is a period of reduced dense water transport until 1999. From 2000 to 2017, a reversal occurs with the transported dense water mass being larger at T5a (reaching $-3.0 \cdot 10^{11}$ kg) compared to T5b ($> -1.0 \cdot 10^{11}$ kg). This may indicate a major change in dense water dynamics over the northern Adriatic shelf – e.g., due to circulation changes or differences between dense water and the ambient water densities and potential shallowing of the dense water outflow – as the dense water arriving through T5b cascades initially to the Jabuka Pit before being transported along the deepest sections of the Palagruža Sill (Vilibić et al., 2004). In contrast, dense waters arriving through T5a are directly coming from the northern Adriatic shelf, detouring the Jabuka Pit along the western shelf.

At T6, in the northwestern part of the southern Adriatic, very large amounts of dense water mass are transported in specific years (1989, 2000, 2002–2006, 2008, 2012, 2013 and

2017), with the largest mass transported in April 2005 reaching -70.0·10$^{11}$ kg. This time series resembles the one at T5a, indicating that most of the dense waters are transported downslope along the western sections of the SAP towards its deeper layers (e.g., Gondola Slide, Bari Canyon, Foglini et al., 2016; Langone et al., 2016).

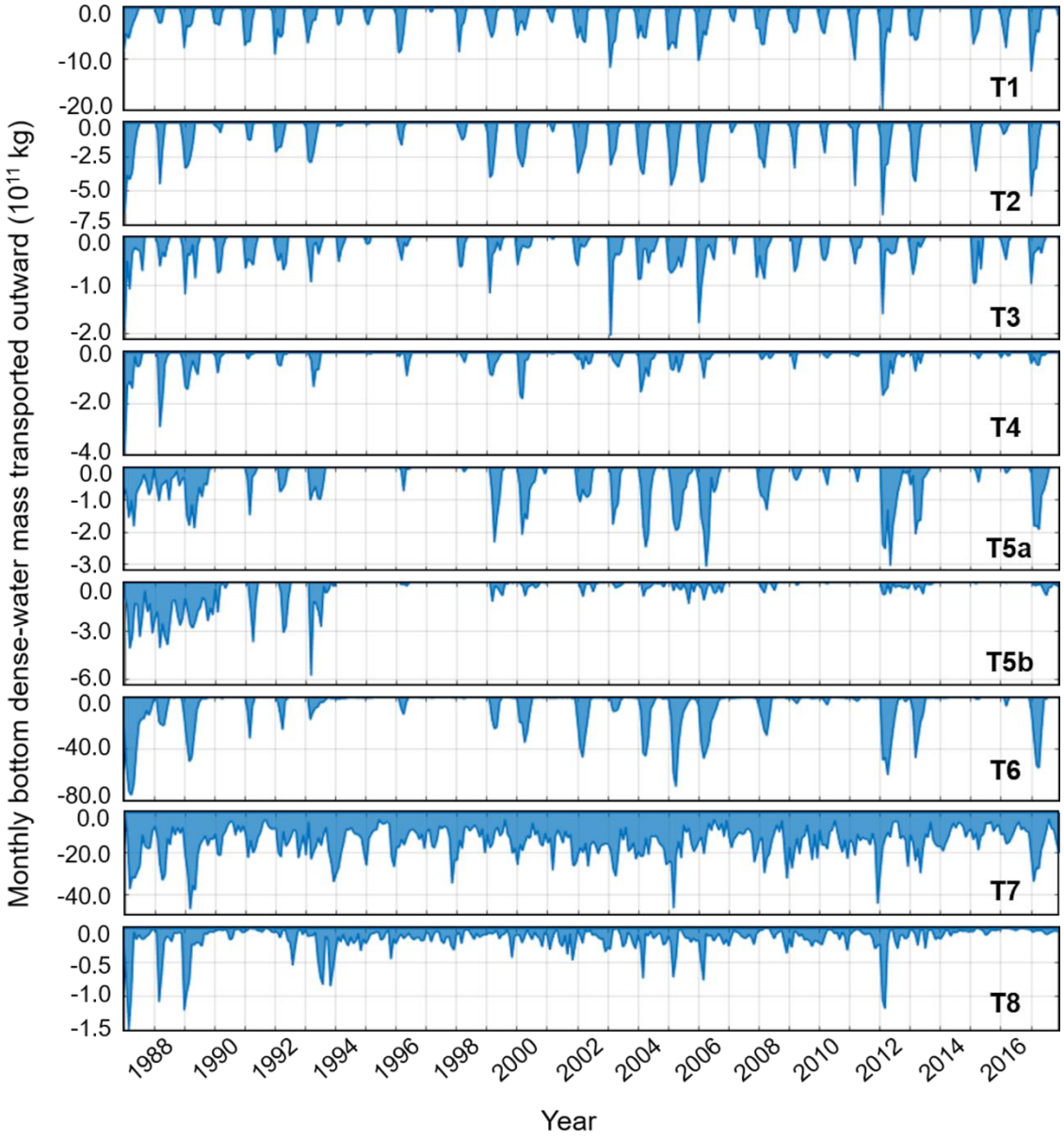


**Figure 4.** Time series of monthly bottom dense water mass transported outward at transects: T1, T2, T3, T4, T5a, T5b, T6, T7 and T8 for the 1987–2017 period.

For transects T1-T6, the AdriSC bottom dense water mass outflows present strong quasi-decadal variations which, as demonstrated in Denamiel et al. (2022), are linked to both the EMT substantially lowering the Adriatic salinities in the 1990s, and the BiOS-driven phases

influencing bottom salinity and ocean current speed variations across the Adriatic basin (e.g., larger dense water mass outflow during the 2000–2006 strong cyclonic BiOS-driven phase).

The remaining transects, T7 and T8, are located in the Strait of Otranto, where T7 is a full-length transect and T8 is a shorter transect covering the shelf on the western coast. The time series reveal completely different dynamics at T7 and T8 compared to the other transects: the dense water transport at T7 is predominantly driven by open-ocean convection in the SAP (e.g., Bensi et al., 2013; Querin et al., 2013), while dense water transport at T8 is also strongly influenced by the properties of the dense water coming over the Palagruža Sill. At least around $-5.0 \cdot 10^{11}$ kg is transported each month through T7 ($-15.0 \cdot 10^{11}$ kg on average), with a few exceptional peaks of $-47.0 \cdot 10^{11}$ kg. At T8, the monthly bottom dense water mass is about $-0.5 \cdot 10^{11}$ kg. In some few years, such as 2012, the values reach $-1.0 \cdot 10^{11}$ kg at the beginning of the year. Notably, the substantial bottom dense water mass outflow in 2012 at T6 and T7 indicates massive dense water production in the northern Adriatic during the winter, being capable to sustain both the strong downslope currents along the western SAP of its denser fraction and strong bottom current along the shelf of its lighter fraction, extending up to the Strait of Otranto. Indeed, a rapid BiOS reversal has been demonstrated after massive dense water outflow in 2012 (Gačić et al., 2014). The same refers to 1987, which is also recognized as a year when massive dense water production was observed (Vilibić and Orlić, 2001). However, in certain years (1992-1993) the dense water outflow at T8 occurs in summer or autumn, indicating that some other mechanism than bottom density current is responsible for transport of these waters.

The monthly climatology of the bottom dense water mass transported outward at the nine transects is examined for the 1987–2017 period (Fig. 5). At T1, the largest amounts of dense water mass are transported from January to April and range from $-2.9 \cdot 10^{11}$ kg (January) to $-5.1 \cdot 10^{11}$ kg (March). Similar distribution is obtained at T2 but with smaller values ranging from $-1.8 \cdot 10^{11}$ to $-2.6 \cdot 10^{11}$ kg. At T3, the transported dense water mass is the largest from February to May, ranging from $-0.2 \cdot 10^{11}$ kg to almost $-0.5 \cdot 10^{11}$ kg, while T4 shows smaller amounts, reaching almost $-0.3 \cdot 10^{11}$ kg.

At T5a, the largest values are obtained in March (approximately $-0.8 \cdot 10^{11}$ kg) and they further decrease until June. The neighbouring transect T5b, shows its largest transported dense water mass in March and May (down to $-0.2 \cdot 10^{11}$ kg), generally having smaller values than T5a. This double maximum may be related to direct outflow over the deepest parts of the Palagruža Sill occurring simultaneously in March, with the outflow along southern sections of the sill (T5a), and a delayed outflow of dense water originating either from old waters residing in the Jabuka Pit or from a spillover of new dense water that first cascade into the pit and then overflow the deepest parts of the Palagruža Sill (May).

Further southeast, at T6, the distribution peaks in March and April, reaching around $-12.0 \cdot 10^{11}$ kg, while in May, it reaches $-4.0 \cdot 10^{11}$ kg, resembling the seasonality reproduced at T5a. Indeed, a delay between bottom dense water mass outflow at T1 and other transects reveals the average time needed for the dense water to travel until it cascades into the SAP. On average, it rapidly reaches the northwestern perimeter of the Jabuka Pit in less than a month, but the Jabuka Pit serves as an obstacle and collector of the densest water, after which the dense water requires an additional month to be transported downslope to the deep SAP (if having sufficiently high

PDA). These modelling results agree with times derived from *in situ* observations (Vilibić and Orlić, 2001).

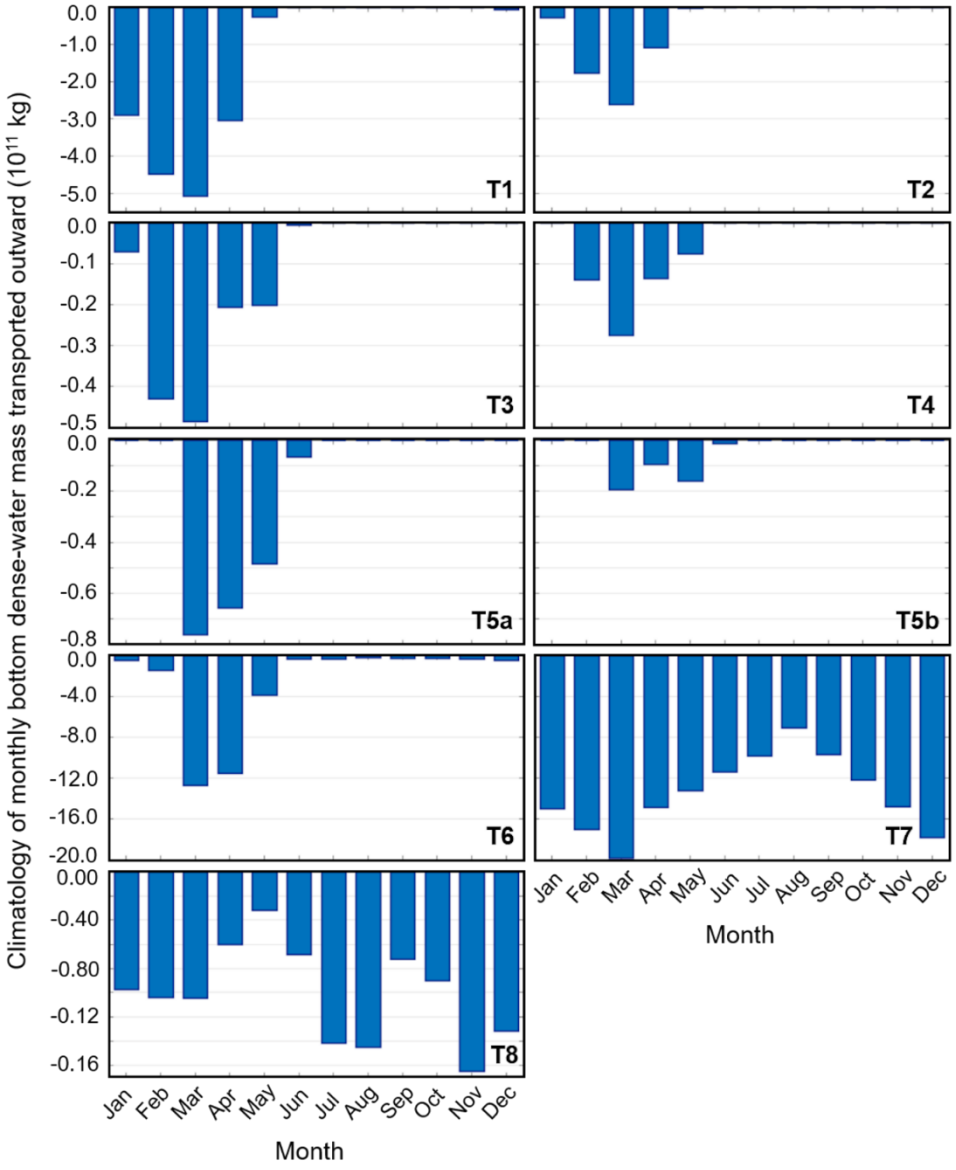


**Figure 5.** Climatology of monthly bottom dense water mass transported outward at transects: T1, T2, T3, T4, T5a, T5b, T6, T7 and T8 for the 1987–2017 period.

At T7, the transported dense water mass remains large throughout the year, increasing from January to March, when it reaches $-20.0 \cdot 10^{11}$ kg, and then decreasing slowly until August down to $-8.2 \cdot 10^{11}$ kg, after which it increases to $-17.8 \cdot 10^{11}$ kg in December. These two maxima may resemble the outflow of dense water after its generation (the March maximum), while the December maximum could result from enhanced circulation and exchange of water masses in the Strait of Otranto, known to occur in late autumn/early winter (e.g., Mihanović et al., 2021). Undoubtedly, the general circulation and water mass exchange between the SAP and the northern Ionian Sea is a driver of the dense water outflow throughout the year, considering the

average capacity of the SAP to accumulate dense water is about two years (Vilibić and Orlić, 2002). Finally, at T8, the bottom dense water mass outflow values remain around $-0.10 \cdot 10^{11}$ kg from January to March, decreasing until May. Larger values are obtained in July and August, reaching down to $-0.14 \cdot 10^{11}$ kg, while the largest transported dense water mass is produced in November ($-0.16 \cdot 10^{11}$ kg) and December ($-0.13 \cdot 10^{11}$ kg).

### 3.3. Accumulation sites

The accumulation of dense water during the 1987-2017 period is first investigated by analysing, in the DKB, JB and DA subdomains, both the animation (Movie S1) of daily time series of bottom PDA and the time series of bottom temperature and salinity (Fig. 6). The general pattern in DKB involves a sharp increase in PDA at the beginning of the year when the dense water generation is occurring and temperatures can drop to 8.5 °C due to consistent wintertime heat losses and cooling events (e.g., Artegiani et al., 1997). It is then followed by a sharp decrease at the end of the year when vertical mixing of the whole water column is occurring in late autumn (e.g., Viličić et al., 2009) and temperatures can reach 17.5 °C. The years with the largest PDAs (> 29.6 kg $m^{-3}$) and lowest winter temperatures (< 10 °C) are: 1993, 2000, 2002, 2004–2006, 2012 (up to 30.0 kg $m^{-3}$) and 2017. Two PDA peaks are frequently occurring during a year, the first in February–March when the dense water formation is occurring, and the second a few months later, during the summer months. The second maximum may resemble either the post-generation spreading of dense water inside the Kvarner Bay associated with a thermohaline circulation due to the dense water sinking from the shallow to the deepest parts of the Kvarner Bay as a slow bottom density current, or the advection of dense water from the northern Adriatic shelf. The bottom salinity variations demonstrate a completely different behaviour as they are mostly driven by the EMT and the BiOS-driven phases as demonstrated in Denamiel et al. (2022): salinities within the 37.9–38.4 range are produced during the 1987–1999 period, followed by a period of larger salinities in the 38.2–38.7 range from 2000–2008 and, after 2008, a short period of smaller salinities occurred from 2009–2011. In 2005, 2012 and 2017, very large salinities surpassing 38.7 coincided with very low temperatures (down to 9 °C), indicating the accumulation of extremely dense waters. Further, the sharp temperature increase in late autumn typically coincides with an increase in salinity, revealing the advection of higher salinity open Adriatic waters in autumn. Salinity is generally dropping during dense water generation, indicating that the generated and advected waters to DKB are coming from shallower regions with more pronounced cooling effects. Finally, as seen in previous studies (Janeković et al., 2014; Pranić et al., 2023), the dense waters reside within the DKB for about a year.

In JP, PDA time series exhibits a “saw-tooth” pattern with large changes occurring every 1–3 years, previously detected in shorter ocean simulations (Mihanović et al., 2018) and observations (Artegiani et al., 2001). This pattern is mostly driven by the temperature variations. During some years (e.g., 2002, 2012), the bottom temperatures present large late-winter decrease resulting from colder dense water cascading into the pit. Conversely, in years lacking this cascading phenomenon (e.g., 2001, 2014), the temperature tends to continue rising. The bottom temperatures mostly vary between 10.5 and 13.5 °C and present the largest drops in 2002 and 2012. In all years except 2012, drops in temperature are associated with drops in salinity, indicating that the dense water generated in the northern Adriatic has lower salinity than the residing waters in the Jabuka Pit. Notably, in 2012, a sharp salinity increase is associated with a sharp decrease in temperature, indicating the arrival of highly saline waters in the northern

Adriatic during autumn 2011, reaching dense water sites in winter 2012. As previously demonstrated, the AdriSC bottom salinity variations within the JP mostly follow the BiOS-driven quasi-decadal oscillations and the influence of the EMT (Denamiel et al., 2022) but also longer positive trends (Tojčić et al., 2023).

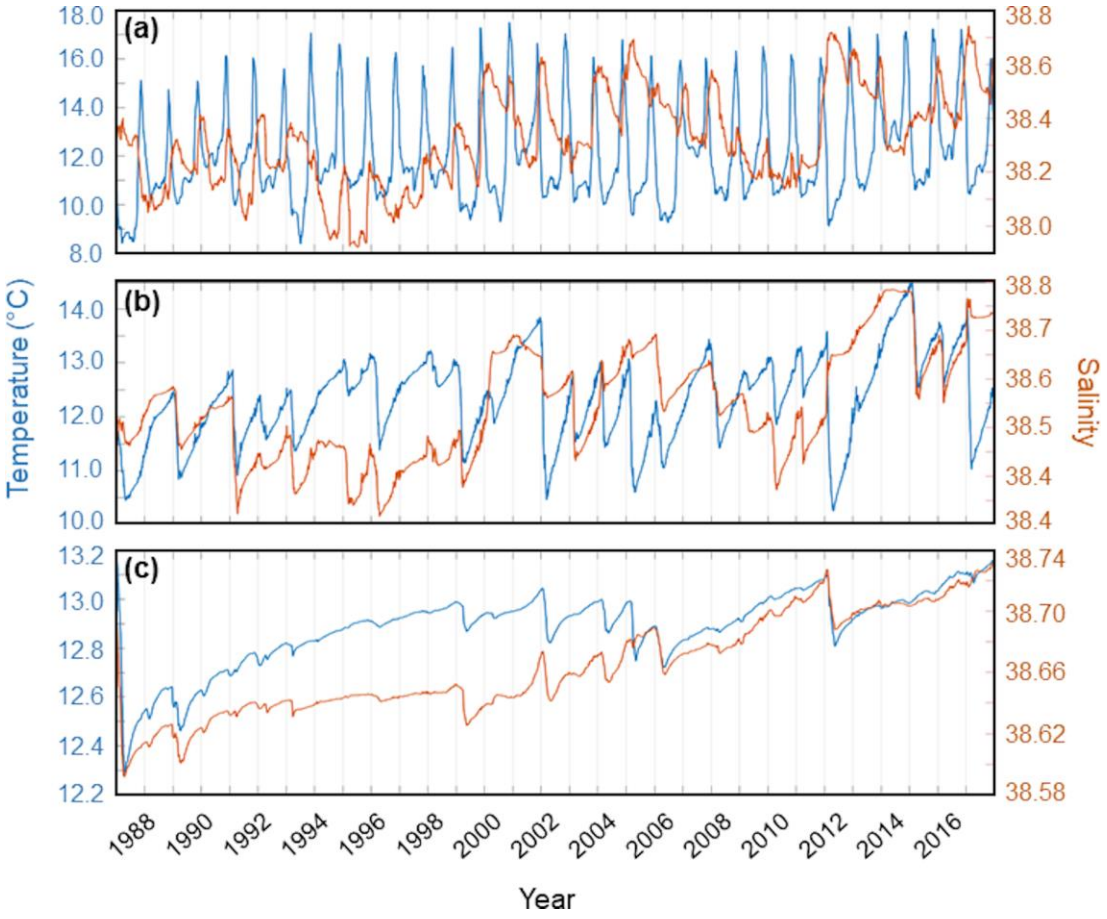


**Figure 6.** Daily time series of bottom temperature and salinity in the (a) deep Kvarner Bay (DKB), (b) Jabuka Pit (JP) and (c) deep Adriatic (DA), during the 1987–2017 period.

In DA, during the 1989–2000 period PDA generally decreased to 29.23 kg $m^{-3}$ with smaller annual variations. After 2000, the PDA slowly increased each year until 2005, when a very sharp rise to 29.30 kg $m^{-3}$ occur. The next sharp increase in the DA bottom PDA values occurred during 2012, reaching slightly less than 29.30 kg $m^{-3}$. Another smaller peak of bottom PDA can be noticed in 2017, restricting the dense water cascading during this event just in the Jabuka Pit, with much lower intensity in the Southern Adriatic Pit. Convincingly, it can be seen that the PDA time series in DA also exhibits a "saw-tooth" pattern already measured by near-bottom sensors at the E2-M3A buoy (Querin et al., 2016), while the AdriSC climate model results indicate large PDA changes occurring there every 5–10 years. Interestingly, the associated bottom temperature and salinity exhibit similar "saw-tooth" patterns. The temperature generally ranges between 12.3 and 13.2 °C, with the largest drops occurring in 2002, 2005 and 2012 when it decreased by slightly more than 0.2 °C during winter. Salinity ranges between 38.60 and 38.73, with several larger jumps such as during 2001–2002, in 2005 and during 2011–

2012. In 2012, in contrast with JP, the decrease in temperature at the bottom of DA is associated with a decrease in salinity.

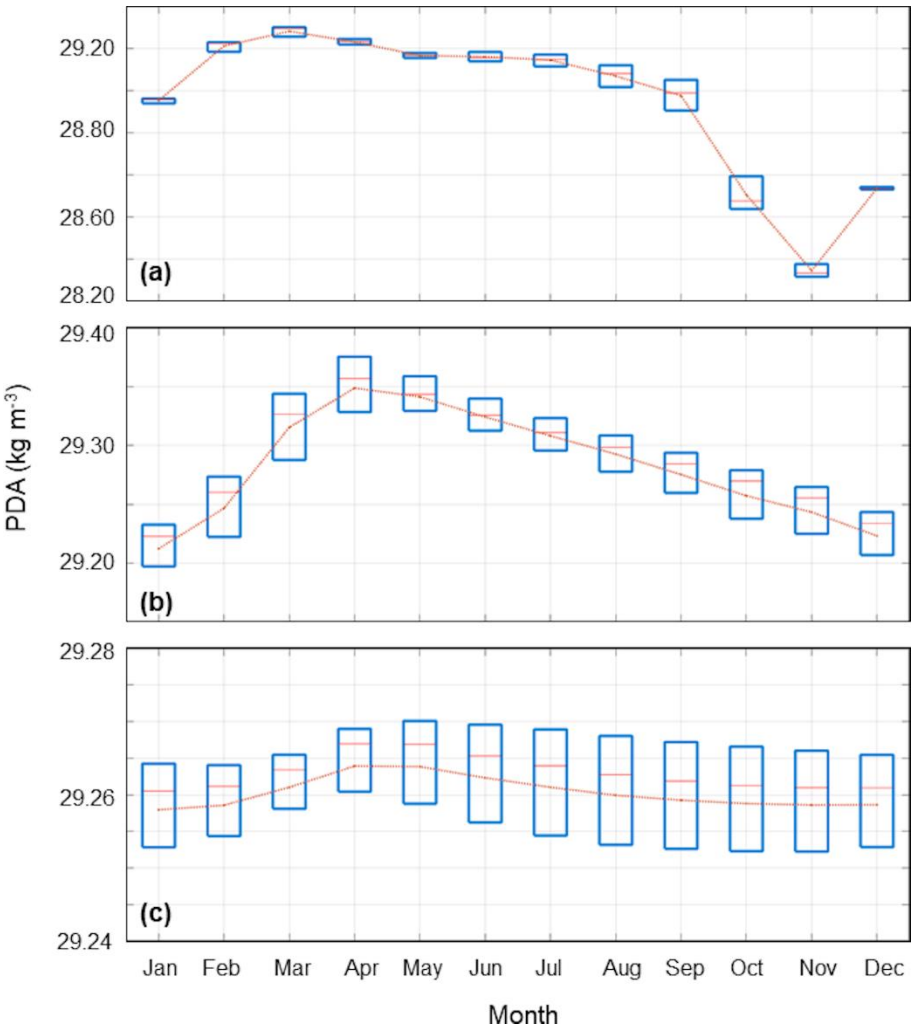


**Figure 7.** Annual courses of monthly box plots of bottom PDA for the (a) deep Kvarner Bay (DKB), (b) Jabuka Pit (JP) and (c) deep Adriatic (DA) subdomain in the 1987–2017 period. The red line inside each box plot denotes the median of the distribution. The orange dotted line connects the mean values of the distributions.

The monthly climatology of bottom PDA for the DKB, JP and DA subdomains is presented in Figure 7, while the corresponding temperature and salinity plots may be found in Supplemental Material (Fig. S5 and S6). In DKB, PDAs are the largest from February to May, peaking in March at around 29.22 kg $m^{-3}$ (Fig. 7a). Then they decrease until May and keep constant values for almost 3 months. This behaviour may result from either a slow dense water spreading from the shallower parts of KB or the advection of dense water from the northern Adriatic shelf. After September, a steep decrease in PDA occur and a minimum of around 28.24 kg $m^{-3}$ is reached in November when the whole water column is mixed. The temperature follows the PDA distributions but in an inverse manner, with a minimum in March down to 10.5 °C and a maximum in November up to 15.7 °C. Salinity shows its largest values in January and

February (around 38.39), after which it decreases, reaching a minimum in October of approximately 38.26, followed by a sharp increase until December and largest variability in November.

In JP, the smallest PDAs are produced in January around 29.3 kg $m^{-3}$, after which there is an increase until April, when they reach around 29.35 kg $m^{-3}$ (Fig. 7b). Therefore, the dense water cascading into the JP lasts from February to April on average. Subsequently, from May to December, PDAs slowly decrease to around 29.23 kg $m^{-3}$, due to the slow mixing with the warmer and more saline intermediate waters. Temperature distributions are very similar to PDA distributions but inversed. Minimum temperatures are reached in April down to 11.7–12.0 °C, after which they increase. Salinities are larger in January and February (around 38.56–38.57) followed by a sharp decrease until May down to 38.52, after which they increase until December, indicating a lag of one month after the temperature changes.

Monthly box plots in DA reveal relatively small variations (Fig. 7c). PDAs slowly increase from February to peak around 29.26 kg $m^{-3}$ in April and May, after which they slightly decrease until the end of the year. Indeed, these distributions indicate the possibility of dense water cascading reaching in average the bottom of the SAP between late February and May. Temperature and salinity have similar behaviour, decreasing until April and May and then slowly increasing until December. The monthly variations in median temperature and salinity are approximately 0.5 °C and slightly larger than 0.01, respectively.

## 4 Discussion

This paper, for the first time, analyses and quantifies the Adriatic multi-decadal bottom dense water dynamics coming from kilometre-scale ocean simulations. For that, the 31-year-long AdriSC atmosphere-ocean historical climate simulation (1987-2017) with horizontal resolution of 1 km has been used. Hereafter, three key results are further discussed and a basic classification of the Adriatic dense water events is proposed.

### 4.1 Dense water generation in the Kvarner Bay

The AdriSC model is the first model to properly simulate the multi-decadal dense water generation within the Kvarner Bay. In particular, in this study, it was found that the differences in maximum PDA during winter months between the open northern Adriatic shelf and the Kvarner Bay dense water generation sites are primarily influenced by a median difference of 2°C in temperature while the salinity difference is neglectable. The difference in temperature between the two generation sites is explained by much larger ocean depths in the Kvarner Bay, so that the cooling rates during severe bora outbreaks – simulated to reach their maximum in the Kvarner Bay by the AdriSC model (Denamiel et al., 2020a, b, 2021a) – are found to be less important for the temperature decrease (and thus, for the PDA increase) than the volume of the ocean to be cooled. However, the fact that no major salinity difference exists between the two generation sites contrasts with previous modelling results. Indeed, the other modelling study spanning over several years – that analysed the results of a ROMS ocean model with a 2 km horizontal resolution forced by 8 km atmospheric fields extracted from the Aladin/HR hydrostatic weather prediction model – found that dense waters generated in the Kvarner Bay were less salty than the dense waters generated on the northern Adriatic shelf (Mihanović et al., 2018). The reason for

the difference in salinity between the two models can be attributed to the several times higher water exchanges between the Kvarner Bay and the open sea reproduced by the AdriSC model (Denamiel et al., 2020b), resulting in faster advection of saline waters from the open sea to the Kvarner Bay. Precisely, it was found during the NAdEx experiment (Vilibić et al., 2018) that the Aladin/HR–ROMS modelling system used by Mihanović et al. (2018) underestimated the transport from and towards the Kvarner Bay by 50% to even 80%, while the evaluation of the AdriSC climate model against available *in situ* observations revealed no substantial biases in the Kvaner Bay (Pranić et al., 2021). Further, previous numerical studies from Denamiel at al. (2021a) and Pranić et al. (2023) demonstrated that, for proper quantification of the dense water generation and water exchanges in the Kvarner Bay, both nonhydrostatic atmospheric models with a maximum resolution of few kilometres and ocean models with at least 1 km resolution should be used in the Adriatic Sea.

The other interesting features of the dense water generation in the Kvaner Bay simulated with the AdriSC model are that it only contributes ca. 25–35% to the overall dense water mass outflow and that a smaller secondary peak in PDA is often found during summer, which is mostly linked to the dynamical behaviour of the deepest Kvarner Bay area as further discussed in section 4.3.

### 4.2 Adriatic basin vs. Otranto Strait mass transports

In the AdriSC historical simulation, the monthly distributions of dense water mass peak in March across most of the Adriatic basin. This result is aligned with previous observational studies that demonstrated that the dense waters generated in the northern Adriatic can travel ca. 200 kilometres southward over 2-3 weeks (Vilibić and Mihanović, 2013) and can influence the thermohaline circulation over the whole Adriatic (Orlić et al., 2007).

In contrasts with the rest of the Adriatic basin dynamical behaviour, the dense water mass transported along the western side of the Otranto Strait (transect T8) presents two maxima in July-August and November-December. The November-December peak is also present along the full Otranto Strait transect (transect T7) and most likely results from enhanced circulation and exchange of water masses in the Strait of Otranto. However, the particular behaviour in July-August is well-illustrated with the animation of the spatial distribution of the PDAs over the Adriatic Sea (Movie S1) that reveals the presence of dense waters (with PDAs >29.4 kg $m^{-3}$ in most years) in July-August along the southwestern Adriatic coast which are fast transported towards the Otranto Strait. This surprising result was never reported in previous observational studies and needs further investigation to understand whether it is linked to a numerical artefact within the AdriSC simulation or realistic dynamical features.

### 4.3 Dynamical behaviour of the accumulation sites

The analysis of the AdriSC model highlights that the dense waters accumulated in the deepest parts of the Kvarner Bay are ventilated annually as the whole bay is regularly mixed during late autumn and winter, while the dense waters accumulated at the bottom of the Jabuka Pit and the Southern Adriatic Pit exhibit “saw-tooth” patterns and are renewed every 1–3 years and every 5–10 years, respectively.

First, the dynamical behaviour of the Kvarner Bay as an accumulation site is primarily linked to its particular geomorphology. Outside of the nearshore areas, most of the depths within the bay are ranging from 60 to 80 m except for a 110-m pit forming the deep Kvarner Bay accumulation area (see the domain outreach in Fig. 1). Consequently, weak bottom density currents are likely to transport the denser waters generated over the shallower regions of the bay towards this pit. As the differences in depth and density between the pit and the rest of the Kvarner Bay are small, this transport is also likely to occur for several weeks or even few months which could explain the presence of a summer peak in the PDA time series extracted over the full Kvarner Bay subdomain. Additionally, dense waters generated over the open northern Adriatic shelf are also being spread towards the Kvarner Bay through connecting channels and may also accumulate in the deepest part of the bay (Vilibić et al., 2018). Second, within the Jabuka Pit accumulation site, the complete ventilation of the whole water column was previously reported to rarely occur (e.g., Bergamasco et al., 1999) which explains the "saw-tooth" pattern simulated with the AdriSC model. Further, new oxygenized waters are almost exclusively coming from dense waters generated yearly in the northern Adriatic (Nof, 1983; Emms, 1997; Artegiani and Salusti, 1987). This explains the synchronization of the year-by-year presence/absence of dense waters within the deep Kvarner Bay and the Jabuka Pit (See Movie S1). Finally, within the Southern Adriatic Pit, dense waters rarely reach the deepest areas of the pit and the renewal of the bottom waters seems to follow the BiOS phases. It is more frequent during the cyclonic BiOS phases (e.g., during the 2000-2006 period as simulated by the AdriSC model; Denamiel et al., 2022) when the advection of more saline waters from the Ionian Sea increases the NAddW density but also lower the stability of the water column and, hence, enhances the AdDW generation (Cardin et al., 2020). In contrast, during the anticyclonic BiOS phases renewal is almost absent (e.g., during the 2007-2011 period as simulated by the AdriSC model; Denamiel et al., 2022) indicating that circulation in the northern Ionian Sea is key for the renewal of the deepest parts of the Adriatic.

### 4.4 Classification of the dense water events

A basic classification of the dense water events was derived from the results of maximum bottom PDA in the northern Adriatic generation site presented in Figure 3, where three catogeries were defined for the box plots: strong (median of maximum PDAs > 30.0 kg $m^{-3}$), moderate (median of maximum PDAs >= 29.5 kg $m^{-3}$ and <= 30.0 kg $m^{-3}$) and weak (median of maximum PDAs < 29.5 kg $m^{-3}$). Spatial distributions of median of the maximum bottom PDAs in the whole Adriatic for the three categories, are shown on Figure 8.

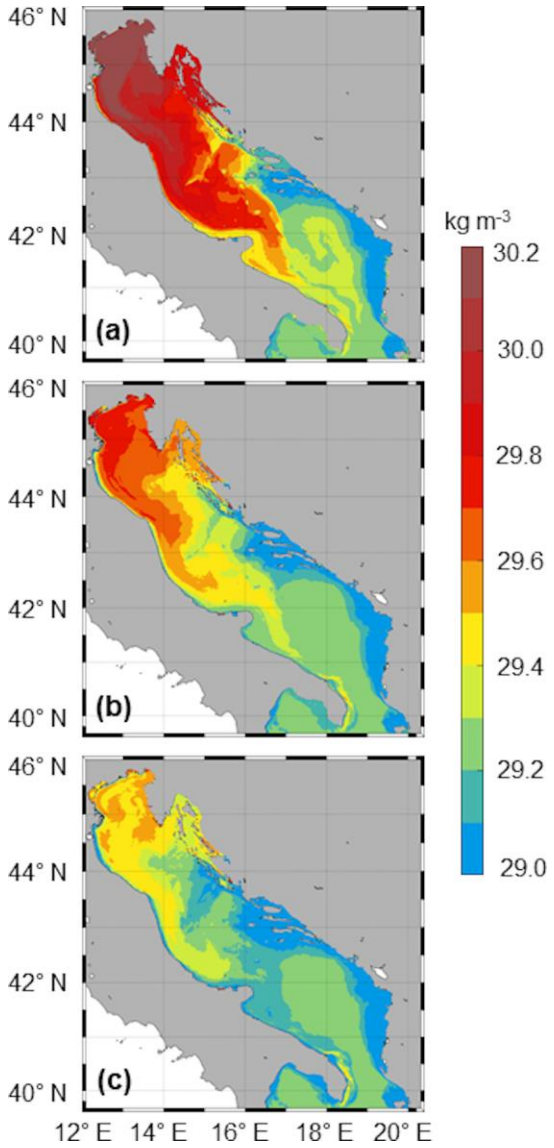


**Figure 8.** Spatial distribution of median maximum bottom PDA for categories of years with (a) strong, (b) moderate, and (c) weak dense water formation, based on the classification of maximum PDA in the northern Adriatic during the JFM period (Figure 3).

In the first category with strong dense water events (Fig. 8a), maximum PDA values surpass 30.0 kg $m^{-3}$ in the whole northern Adriatic and reach up to 30.0 kg $m^{-3}$ in the Kvarner Bay and middle Adriatic. Large PDAs are also present in the Jabuka Pit and along the western coast towards the SAP, where an inflow of bottom dense water with PDA up to 29.4 kg $m^{-3}$ can be noticed, cascading to the bottom SAP layers and forming the near-bottom cyclonic gyre. As the near-bottom dense waters need about a month to encircle the SAP (Movie S1), their speed may be estimated to ca. 15 cm $s^{-1}$ before fully filling the SAP bottom. The second category with moderate dense water events (Fig. 8b), is characterized by maximum PDAs up to 29.8 kg $m^{-3}$ in the northwestern part of the northern Adriatic and up to 29.7 kg $m^{-3}$ in the southeastern part of the northern Adriatic and along the western side of the middle Adriatic. In the Kvarner Bay, the values are mostly between 29.5 and 29.6 kg $m^{-3}$, while in the Jabuka Pit they reach up to 29.5 kg

$m^{-3}$. Here, an outflow of dense water is still present along the western coast, while the PDA in the SAP reaches up to 29.3 kg $m^{-3}$ with little to no dense water cascading reproduced by the model. The third category of years with weak dense water formation (Fig. 8c) shows larger maximum PDAs only in some parts of the northern Adriatic (up to 29.6 kg $m^{-3}$), while in the Kvarner Bay and middle Adriatic values mostly reach up to 29.5 kg $m^{-3}$. There is some transport along the western side of the middle Adriatic, while in the Jabuka Pit and SAP the values are mostly uniform up to 29.3 kg $m^{-3}$ as no dense water cascading occurs in both accumulation sites.

The classification of dense water generation events exhibits common spatial patterns in bottom maximum PDA, while mainly differing in magnitude. To obtain more details on the similarities and differences in the dense water outflow, additional research should be performed using not just bottom density data but also currents over the whole water column.

## 5 Conclusions

In this study, the AdriSC climate model has been used to numerically assess, for the very first time, the Adriatic dense water multi-decadal dynamical properties at 1-km horizontal resolution. In contrast with previous numerical simulations used in the Adriatic Sea, the presented results have been demonstrated to be aligned with the known literature mostly relying on observational studies. Consequently, the AdriSC far-future RCP 8.5 climate simulation (2070-2100 period) can now be used to assess the impact of extreme climate warming on the Adriatic thermohaline circulation. An analysis of trends, variability and extreme events based on this AdriSC far-future simulation (Tojčić et al., 2024) has already demonstrated that the dense water formation in the northern Adriatic is likely to be reduced while the southern Adriatic cyclonic gyre is likely to intensify and shrink, and the vertical stratification in the deepest part of the Adriatic is likely to strengthen. As similar results were also found by Parras-Berrocal et al. (2023) using one member of the Med-CORDEX ensemble (Ruti et al., 2016), further analyses of the kilometre-scale atmosphere-ocean AdriSC far-future climate simulation must now be performed and might provide a new vision of the Adriatic dense water dynamical properties under extreme warming.

## Acknowledgments

The computing and archive facilities used in this research were provided by the European Centre for Medium-range Weather Forecasts (ECMWF) through national quota and the ECMWF Special Projects ‘The Adriatic decadal and inter-annual oscillations: modelling component’ and ‘Numerical modelling of the Adriatic-Ionian decadal and inter-annual oscillations: from realistic simulations to process-oriented experiments’. The research has been supported by the Croatian Science Foundation projects ADIOS (Grant IP-06-2016-1955), BivACME (Grant IP-2019-04-8542), C3PO (Grant IP-2022-10-9139) and GLOMETS (Grant IP-2022-10-306), the HORIZON EUROHPC JU project ChEESE-2P (Grant 101093038), as well as the project of Institute of Oceanography and Fisheries (Split, Croatia) KLIMADRIA.

## Data Availability Statement

The code of the COAWST model as well as the ecFlow pre-processing scripts and the input data needed to re-run the AdriSC climate model in evaluation mode can be obtained under the Open Science Framework (OSF) data repository (Denamiel, 2021) under the MIT license.
The model results used to produce this article can be obtained under the Open Science Framework (OSF) FAIR data repository (Pranić, 2024).

## References

Artegiani, A. & Salusti, E. (1987), Field observation of the flow of dense water on the bottom of the Adriatic Sea during the winter of 1981. Oceanologica Acta, 10, 387-391.

Artegiani, A., Bregant, D., Paschini, E., Pinardi, N., Raicich, F., & Russo, A. (1997), The Adriatic Sea general circulation, part I: air-sea interactions and water mass structure, Journal of Physical Oceanography, 27, 1492–1514. doi:10.1175/1520-0485(1997)027<1492:TASGCP>2.0.CO;2

Artegiani, A., Marini, M., Pariante, R., Paschini, E., & Russo, A. (2001), Evolution of physical parameters and chemical observations in the Middle Adriatic depressions. Archo Oceanography Limnolology, 22, 27-34.

Batistić, M., Garić, R., & Molinero, J.C. (2004), Interannual variations in Adriatic Sea zooplankton mirror shifts in circulation regimes in the Ionian Sea. Climate Research, 61, 231-240. doi:10.3354/cr01248

Belušić, D., & Klaić, Z. B. (2004), Estimation of bora wind gusts using a limited area model. Tellus, 56, 296–307, doi:10.1111/j.1600-0870.2004.00068.x

Bensi, M., Cardin, V., Rubino, A., Notarstefano, G., & Poulain, P.M. (2013), Effects of winter convection on the deep layer of the Southern Adriatic Sea in 2012. Journal of Geophysical Research: Oceans, 118, 6064-6075, doi:10.1002/2013JC009432

Bergamasco, A., Oguz, T., & Malanotte-Rizzoli, P. (1999), Modeling dense water mass formation and winter circulation in the northern and central Adriatic Sea. J. Mar. Syst., 20, 279–300. doi:10.1016/S0924-7963(98)00087-6

Boldrin, A., Carniel, S., Giani, M., Marini, M., Bernardi Aubry, F., Campanelli, A., Grilli, F., & Russo, A. (2009), Effects of bora wind on physical and biogeochemical properties of stratified waters in the northern Adriatic. Journal of Geophysical Research, 114, C08S92, doi:10.1029/2008JC004837

Bowman, A. W., & Azzalini, A. (1997), Applied Smoothing Techniques for Data Analysis. New York: Oxford University Press Inc., ISBN 0191545694.

Cardin, V., Wirth, A., Khosravi, M., & Gačić, M. (2020), South Adriatic recipes: Estimating the vertical mixing in the deep pit. Frontiers in Marine Science, 7, 565982, doi:10.3389/fmars.2020.565982

669 Civitarese, G., Gačić, M., Batistić, M., Bensi, M., Cardin, V., Dulčić, J., Garić, R., & Menna, M.
670 (2023), The BiOS mechanism: History, theory, implications. Progress in Oceanography, 216,
671 103056. doi:10.1016/j.pocean.2023.10305

672 Denamiel, C. L. (2021), AdriSC Climate Model: Evaluation Run. OSF [code],
673 doi:10.17605/OSF.IO/ZB3CM

674 Denamiel, C., Šepić, J., Ivanković, D., & Vilibić, I. (2019), The Adriatic Sea and Coast
675 modelling suite: Evaluation of the meteotsunami forecast component. Ocean Modelling, 135,
676 71–93. doi:10.1016/j.ocemod.2019.02.003

677 Denamiel, C., Tojčić, I., & Vilibić, I. (2020a), Far future climate (2060–2100) of the northern
678 Adriatic air–sea heat transfers associated with extreme bora events. Climate Dynamics, 55,
679 3043–3066. doi:10.1007/s00382-020-05435-8

680 Denamiel, C., Pranić, P., Quentin, F., Mihanović, H., & Vilibić, I. (2020b), Pseudo-global
681 warming projections of extreme wave storms in complex coastal regions: The case of the
682 Adriatic Sea. Climate Dynamics, 55, 2483–2509. doi:10.1007/s00382-020-05397-x

683 Denamiel, C., Tojčić, I., & Vilibić, I. (2021a), Balancing accuracy and efficiency of atmospheric
684 models in the northern Adriatic during severe bora events. Journal of Geophysical Research:
685 Oceans, 126, e2020JD033516. doi:10.1029/2020JD033516

686 Denamiel, C., Pranić, P., Ivanković, D., Tojčić, I., & Vilibić, I. (2021b), Performance of the
687 Adriatic Sea and Coast (AdriSC) climate component—a COAWST V3.3-based coupled
688 atmosphere-ocean modelling suite: atmospheric dataset. Geoscientific Model Development, 14,
689 3995–4017. doi:10.5194/gmd-14-3995-202127

690 Denamiel, C., Tojčić, I., Pranić, P., & Vilibić, I. (2022), Modes of the BiOS-driven Adriatic Sea
691 thermohaline variability. Climate Dynamics, 59, 1097–1113, doi:10.1007/s00382-022-06178-4

692 Dorman, C. E., Carniel, S., Cavaleri, L., Sclavo, M., Chiggiato, J., Doyle, J., Haack, T., Pullen,
693 J., Grbec, B., Vilibić, I., Janeković, I., Lee, C., Malačić, V., Orlić, M., Paschini, E., Russo, A.,
694 &Signell, R. P. (2007), Winter 2003 marine atmospheric conditions and the bora over the
695 northern Adriatic. Journal of Geophysical Research: Oceans, 112, C03S03.
696 doi:10.1029/2005JC003134

697 Dukowicz, J. K. (2001), Reduction of pressure and pressure gradient errors in ocean simulations.
698 Journal of Physical Oceanography, 31, 1915–1921. doi:10.1175/1520-
699 0485(2001)031<1915:RODAPG>2.0.CO;2

700 Dunić, N., Vilibić, I., Šepić, J., Mihanović, H., Sevault, F., Somot, S., Waldman, R., Nabat, P.,
701 Arsouze, T., Pennel, R., Jordà, J., & Precali, R. (2019), Performance of multi-decadal ocean
702 simulations in the Adriatic Sea. Ocean Modelling, 134, 84-109.
703 doi:10.1016/j.ocemod.2019.01.006

704 Emms, P.W. (1997), Streamtube models of gravity currents in the ocean. Deep-Sea Research I,
705 44, 1575–1610. doi:10.1016/S0967-0637(97)00047-2

706 Foglini, F., Campiani, E., & Trincardi, F. (2016), The reshaping of the South West Adriatic
707 Margin by cascading of dense shelf waters, Marine Geology., 375, 64–81.
708 doi:10.1016/j.margeo.2015.08.011

709 Gačić, M., Civitarese, G., Miserocchi, S., Cardin, V., Crise, A., & Mauri, E. (2002), The open-
710 ocean convection in the Southern Adriatic: a controlling mechanism of the spring phytoplankton
711 bloom. Continental Shelf Research, 22, 1897-1908. doi:10.1016/S0278-4343

712 Gačić, M., Borzelli, G. E., Civitarese, G., Cardin, V., & Yari, S. (2010), Can internal processes
713 sustain reversals of the ocean upper circulation? The Ionian Sea example. Geophysical Research
714 Letters, 37(9). doi:10.1029/2010GL043216

715 Gačić, M., Civitarese, G., Kovačević, V., Ursella, L., Bensi, M., Menna, M., Cardin, V., Poulain,
716 P.-M., Cosoli, S., Notarstefano, G., & Pizzi, C. (2014), Extreme winter 2012 in the Adriatic: an
717 example of climatic effect on the BiOS rhythm. Ocean Science, 10, 513–522. doi:10.5194/os-10-
718 513-2014

719 Janeković, I., Mihanović, H., Vilibić, I., & Tudor, M. (2014), Extreme cooling and dense water
720 formation estimates in open and coastal regions of the Adriatic Sea during the winter of 2012. J.
721 Geophysical Research: Oceans, 119, 3200–3218. doi:10.1002/ 2014JC009865

722 Jasprica, N., Čalić, M., Kovačević, V., Bensi, M., Dupčić Radić, I., Garić, R., & Batistić, M.
723 (2022), Phytoplankton distribution related to different winter conditions in 2016 and 2017 in the
724 open southern Adriatic Sea (eastern Mediterranean). Journal of Marine Systems, 226, 103665.
725 doi:10.1016/j.jmarsys.2021.103665

726 Laprise, R. (1992), The Euler Equations of motion with hydrostatic pressure as independent
727 variable, Monthly Weather Reviews, 120, 197–207. doi:10.1175/1520-
728 0493(1992)120<0197:TEEOMW>2.0.CO;2.

729 Langone, L., Conese, I., Miserocchi, S., Boldrin, A., Bonaldo, D., Carniel, S., Chiggiato, J.,
730 Turchetto, M., Borghini, M., & Tesi, T. (2016), Dynamics of particles along the western margin
731 of the Southern Adriatic: Processes involved in transferring particulate matter to the deep basin.
732 Marine Geology, 375, 28–43. doi:10.1016/j.margeo.2015.09.004

733 Levitus, S., & Boyer, T.P. (1994a), World Ocean Atlas 1994, Volume 4: Temperature, NOAA
734 Atlas NESDIS 4, US Dept. of Commerce.

735 Levitus, S., Burgett, R., & Boyer, T.P. (1994b), World Ocean Atlas 1994, Volume 3: Salinity,
736 NOAA Atlas NESDIS 3, US Dept. Commerce.

737 Ličer, M., Smerkol, P., Fettich, A., Ravdas, M., Papapostolou, A., Mantziafou, A., Strajnar, B.,
738 Cedilnik, J., Jeromel, M., Jerman, J., Petan, S., Malačič, V., & Sofianos, S. (2016), Modeling the
739 ocean and atmosphere during an extreme bora event in northern Adriatic using one-way and two-
740 way atmosphere–ocean coupling. Ocean Science, 12, 71-86. doi:10.5194/os-12-71-2016

741 Mantziafou, A., & Lascaratos, A. (2008), Deep-water formation in the Adriatic Sea: interannual
742 simulations for the years 1979–1999. Deep–Sea Research I, 55, 1403–1427.
743 doi:10.1016/j.dsr.2008.06.005

744 Mihanović, H., Vilibić, I., Carniel, S., Tudor, M., Russo, A., Bergamasco, A., Bubić, N.,
745 Ljubešić, Z., Viličić, D., Boldrin, A., Malačić, V., Celio, M., Comici, C., & Raicich, F. (2013),
746 Exceptional dense water formation on the Adriatic shelf in the winter of 2012. Ocean Science, 9,
747 561–572. doi:10.5194/os-9-561-2013

748 Mihanović, H., Janeković, I., Vilibić, Bensi, M., & Kovačević, V. (2018), Modelling interannual
749 changes in dense water formation on the northern Adriatic shelf. Pure and Appl. Geophysics,
750 175, 4065–4081. doi:10.1007/s00024-018-1935-5

751 Mihanović, H., Vilibić, I., Šepić, J., Matić, F., Ljubešić, Z., Mauri, E., Gerin, R., Notarstefano,
752 G., & Poulain, P.-M. (2021), Observation, preconditioning and recurrence of exceptionally high
753 salinities in the Adriatic Sea. Frontiers in Marine Science, 8, 672210.
754 doi:10.3389/fmars.2021.672210

755 Nof, D. (1983), The translation of isolated cold eddies along a sloping bottom. Deep-Sea
756 Research, 30, 171–182. doi:10.1016/0198-0149(83)90067-5

757 Oddo, P., & Guarnieri, A. (2011), A study of the hydrographic conditions in the Adriatic Sea
758 from numerical modelling and direct observations (2000–2008). Ocean Science, 7, 549-567,
759 doi:10.5194/os-7-549-2011

760 Orlić, M., Dadić, V., Grbec, B., Leder, N., Marki, A., Matić, F., Mihanović, H., Beg Paklar, G.,
761 Pasarić, M., Pasarić, Z., & Vilibić, I. (2007), Wintertime buoyancy forcing, changing seawater
762 properties and two different circulation systems produced in the Adriatic. Journal of Geophysical
763 Research: Oceans, 112, C03S07. doi:10.1029/2005JC003271

764 Paladini de Mendoza, F., Schroeder, K., Langone, L., Chiggiato, J., Borghini, M., Giordano, P.,
765 Verazzo, G., Miserocchi, S. (2022), Deep-water hydrodynamic observations of two moorings
766 sites on the continental slope of the southern Adriatic Sea (Mediterranean Sea). Earth System
767 Science Data, 14, 5617-5635. doi:10.5194/essd-14-5617-2022

768 Parras-Berrocal, I. M., Vázquez, R., Cabos, W., Sein, D. V., Álvarez, O., Bruno, M., &
769 Izquierdo, A. (2023), Dense water formation in the eastern Mediterranean under a global
770 warming scenario. Ocean Science, 19, 941–952. doi:10.5194/os-19-941-2023

771 Pranić, P. (2024), Kilometre-Scale Climatology of the Adriatic Dense Water. OSF [dataset].

772 Pranić, P., Denamiel, C., & Vilibić, I. (2021), Performance of the Adriatic Sea and Coast
773 (AdriSC) climate component—a COAWST V3.3-based one-way coupled atmosphere–ocean
774 modelling suite: ocean results. Geoscientific Model Development, 14, 5927–5955.
775 doi:10.5194/gmd-14-5927-2021

776 Pranić, P., Denamiel, C., Janeković, I., & Vilibić, I. (2023), Multi-model analysis of Adriatic
777 dense-water dynamics. Ocean Science, 19, 649–670. doi:10.5194/os-19-649-2023

778 Querin, S., Bensi, M., Cardin, V., Solidoro, C., Bacer, S., Mariotti, L., Stel, F., & Malačič, V.
779 (2016), Saw-tooth modulation of the deep-water thermohaline properties in the southern Adriatic
780 Sea. J. Geophys. Res. Oceans, 121, 4585-4600. doi:10.1002/2015JC011522

781 Raicich, F., Malačić, V., Celio, M., Giaiotti, D., Cantoni, C., Colucci, R.R., Čermelj, B., &
782 Pucillo, A. (2013), Extreme air–sea interactions in the Gulf of Trieste (North Adriatic) during the
783 strong Bora event in winter 2012. Journal of Geophysical Research, 118, 5238–5250,
784 doi:10.1002/jgrc.20398

785 Roether, W., Klein, B., Manca, B.B., Theocharis, A., Kioroglou, S. (2007), Transient Eastern
786 Mediterranean deep waters in response to themassive dense-water output of the Aegean Sea in
787 the 1990's. Progress in Oceanography 74:540–571, doi:10.1016/j.pocean.2007.03.001

788 Ruti, P., Somot, S., Giorgi, F., Dubois, C., Flaounas, E., Obermann, A., et al. (2016), Med-
789 CORDEX initiative for Mediterranean climate studies. Bulletin of American Meteorological
790 Society, 97, 1187-1208. doi:10.1175/ BAMS-D-14-00176.1

791 Shchepetkin, A.F., & McWilliams, J.C. (2009), Correction and commentary for "Ocean
792 forecasting in terrain-following coordinates: Formulation and skill assessment of the regional
793 ocean modeling system" by Haidvogel et al., Journal of Computational Physics, 227, pp. 3595–
794 3624, Journal of Computational Physics 228, 8985–9000. doi:10.1016/j.jcp.2009.09.002

795 Skamarock, W. C., Klemp, J. B., Dudhia, J., Gill, D. O., Barker, D. M., Wang, W., & Powers, J.
796 G. (2005), A description of the Advanced Research WRF Version 2, NCAR Technical Note
797 NCAR/TN468+STR, doi:10.5065/D6DZ069T

798 Tojčić, I., Denamiel, C., & Vilibić, I. (2023), Kilometer-scale trends and variability of the
799 Adriatic present climate (1987–2017). Climate Dynamics, 61, 2521–2545. doi:10.1007/s00382-
800 023-06700-2

801 Tojčić, I., Denamiel, C., & Vilibić, I. (2024), Kilometer-scale trends, variability, and extremes of
802 the Adriatic far-future climate (RCP 8.5, 2070−2100). Frontiers in Marine Science, 11, 1329020.
803 doi:fmars.2024.1329020

804 Vilibić, I. & Orlić, M. (2001), Least squares tracer analysis of water masses in the South Adriatic
805 (1967–1990). Deep-Sea Research I, 48, 2297–2330. doi:10.1016/S0967-0637(01)00014-0

806 Vilibić, I., & Orlić, M. (2002), Adriatic water masses, their rates of formation and transport
807 through the Otranto Strait. Deep-Sea Research I, 49, 1321-1340. doi:10.1016/S0967-
808 0637(02)00028-6

809 Vilibić, I. Grbec, B., & Supić, N. (2004), Dense water generation in the north Adriatic in 1999
810 and its recirculation along the Jabuka Pit. Deep-Sea Research I, 51, 1457-1474.
811 doi:10.1016/j.dsr.2004.07.012

812 Vilibić, I., Beg Paklar, G., Žagar, N., Mihanović, H., Supić, N., Žagar, M., Domijan, N., &
813 Pasarić, M. (2008), Summer breakout of trapped bottom dense water from the northern Adriatic.
814 Journal of Geophysical Research: Oceans, 113, C11S02. doi:10.1029/2007JC004535

815 Vilibić, I., & Mihanović, H. (2015), Observing the bottom density current over a shelf using an
816 Argo profiling float. Geophysical Research Letters, 40, 910–915, doi:10.1002/grl.50215

817 Vilibić, I., Mihanović, H., Janeković, I., Denamiel, C., Poulain, P.-M., Orlić, M., Dunić, N.,
818 Dadić, V., Pasarić, M., Muslim, S., Gerin, R., Matić, F., Šepić, J., Mauri, E., Kokkini, Z., Tudor,
819 M., Kovač, Ž., & Džoić, T. (2018), Wintertime dynamics in the coastal northeastern Adriatic
820 Sea: the NAdEx 2015 experiment. Ocean Science, 14. doi:10.5194/os-14-237-2018, 237-258

821 Vilibić, I., Pranić, P., & Denamiel, C. (2023), North Adriatic Dense Water: lessons learned since
822 the pioneering work of Mira Zore-Armanda 60 years ago. Acta Adriatica, 38, 100527.
823 doi:10.32582/aa.64.1.11

824 Viličić, D., Kuzmić, M., Bosak, S., Šilović, T., Hrustić, E., & Burić, Z. (2009), Distribution of
825 phytoplankton along the thermohaline gradient in the north-eastern Adriatic channel; winter
826 aspect. Oceanologia, 51, 495-513. doi:10.5697/oc.51-4.495

827 Warner, J. C., Armstrong, B., He, R., & Zambon, J. B. (2010), Development of a Coupled
828 Ocean-Atmosphere-Wave-Sediment Transport (COAWST) modeling system. Ocean Modelling,
829 35, 230–244. doi :10.1016/j.ocemod.2010.07.010

830 Zore-Armanda, M. (1963), Les masses d'eau de la mer Adriatique. Acta Adriatica, 10, 5–88.

**Figure 1.**

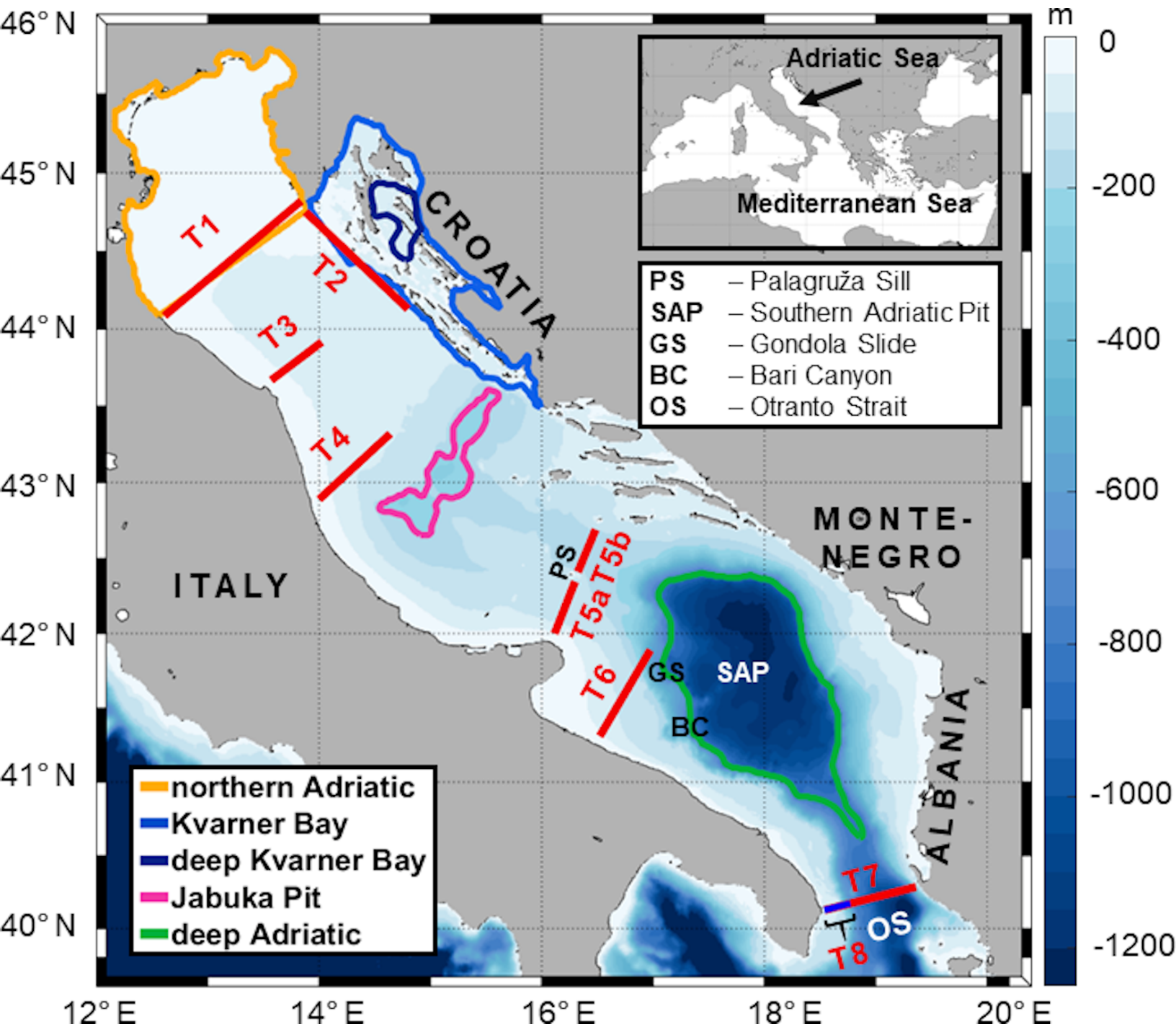
46° N
45° N
44° N
43° N
42° N
41° N
40° N
12° E
14° E
16° E
18° E
20° E
m
0
-200
-400
-600
-800
-1000
-1200
Adriatic Sea
Mediterranean Sea
PS – Palagruža Sill
SAP – Southern Adriatic Pit
GS – Gondola Slide
BC – Bari Canyon
OS – Otranto Strait
T1
T2
T3
T4
T5a T5b
T6
T7
T8
PS
GS
SAP
BC
OS
CROATIA
ITALY
MONTE-
NEGRO
ALBANIA
northern Adriatic
Kvarner Bay
deep Kvarner Bay
Jabuka Pit
deep Adriatic

**Figure 2.**

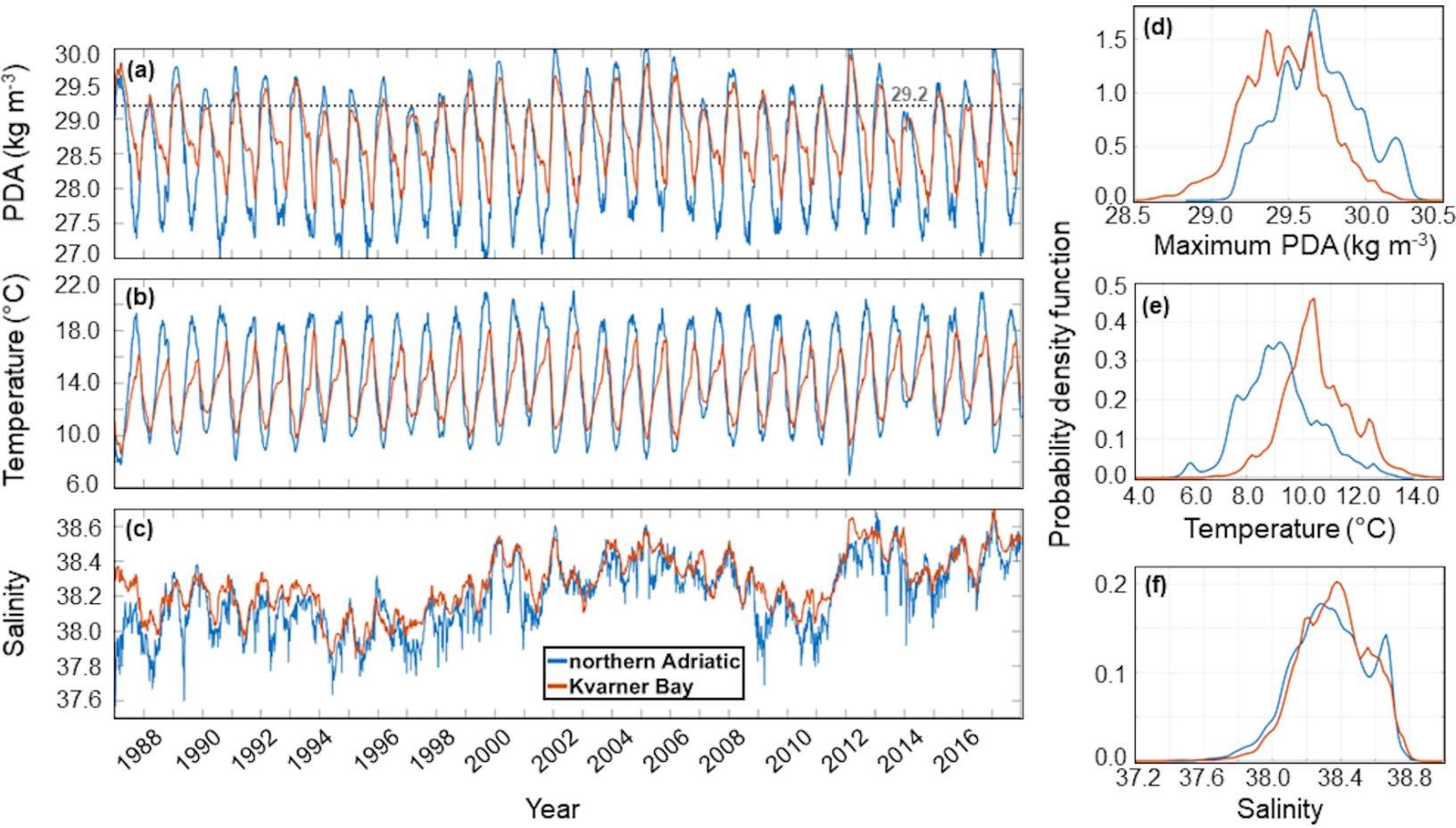
(a)
(b)
(c)
(d)
(e)
(f)
PDA (kg m-3)
Temperature (°C)
Salinity
29.2
northern Adriatic
Kvarner Bay
Year
Probability density function
Maximum PDA (kg m-3)
Temperature (°C)
Salinity

**Figure 3.**

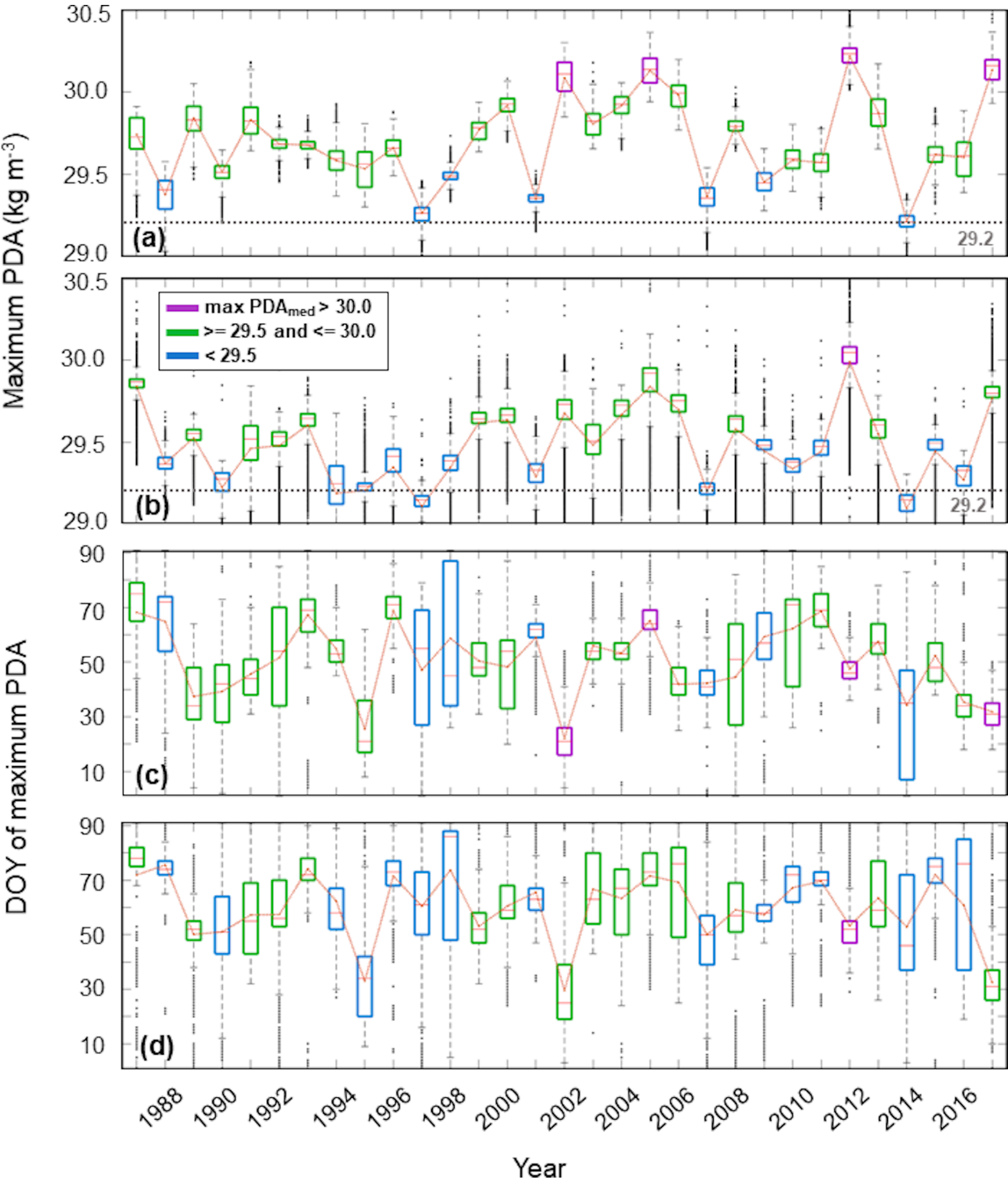
Maximum PDA (kg m-3)
30.5
30.0
29.5
29.0
(a)
29.2
(b)
max PDAmed > 30.0
>= 29.5 and <= 30.0
< 29.5
DOY of maximum PDA
90
70
50
30
10
(c)
(d)
1988
1990
1992
1994
1996
1998
2000
2002
2004
2006
2008
2010
2012
2014
2016
Year

**Figure 4.**

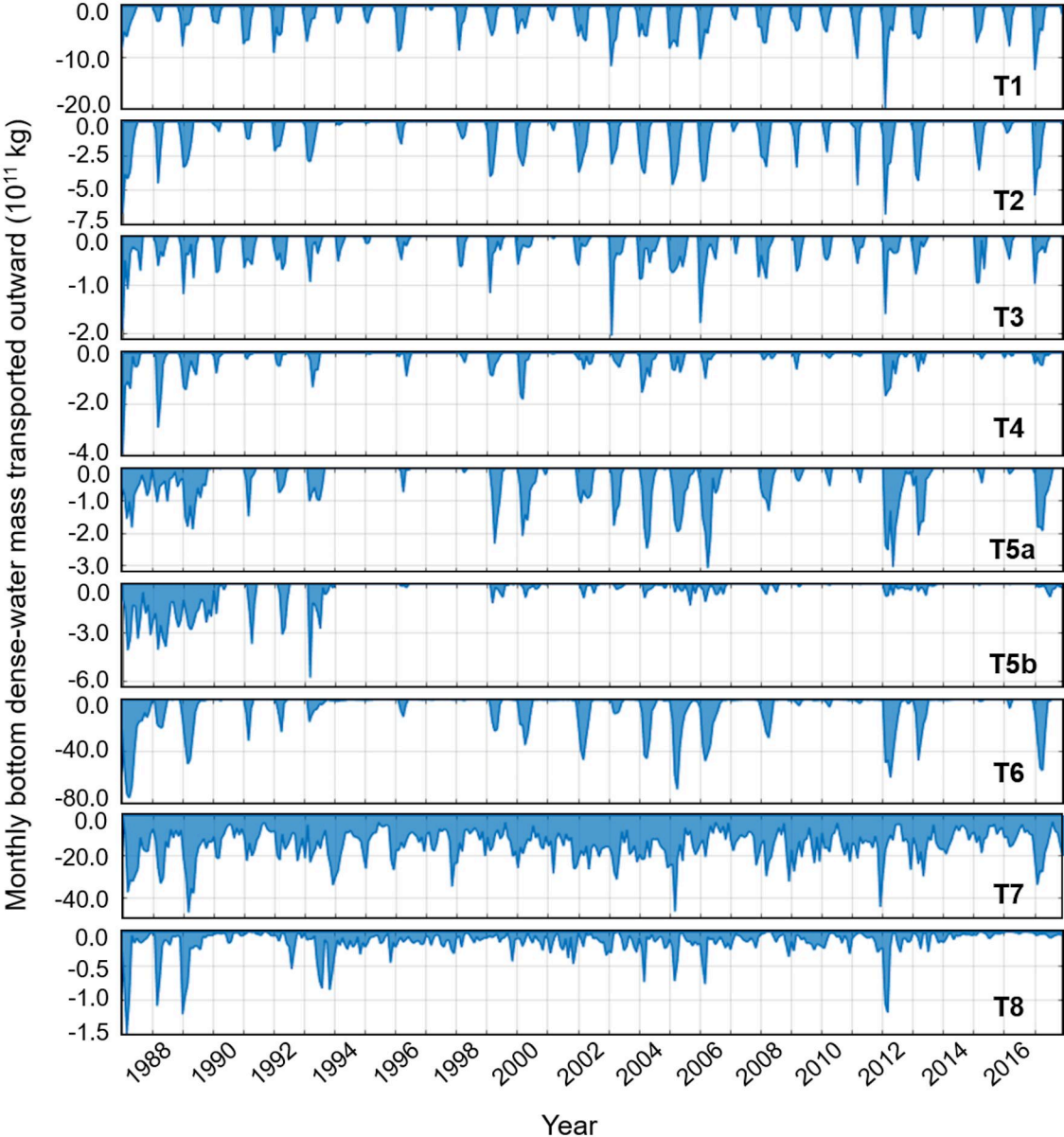
Monthly bottom dense-water mass transported outward ($10^{11}$ kg)
0.0
-10.0
-20.0
T1
0.0
-2.5
-5.0
-7.5
T2
0.0
-1.0
-2.0
T3
0.0
-2.0
-4.0
T4
0.0
-1.0
-2.0
-3.0
T5a
0.0
-3.0
-6.0
T5b
0.0
-40.0
-80.0
T6
0.0
-20.0
-40.0
T7
0.0
-0.5
-1.0
-1.5
T8
1988
1990
1992
1994
1996
1998
2000
2002
2004
2006
2008
2010
2012
2014
2016
Year

**Figure 5.**

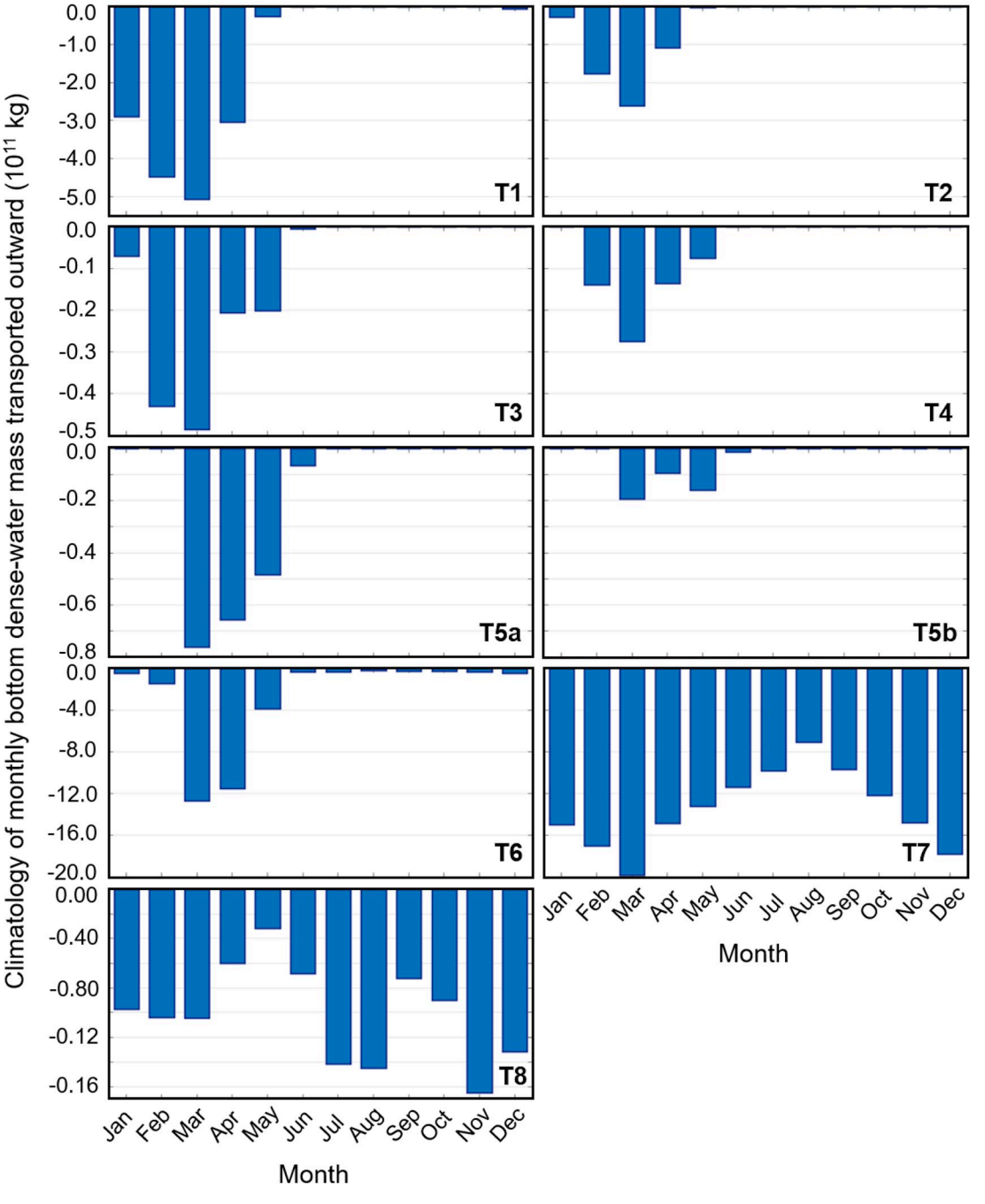
Climatology of monthly bottom dense-water mass transported outward ($10^{11}$ kg)
T1
T2
T3
T4
T5a
T5b
T6
T7
T8
Jan
Feb
Mar
Apr
May
Jun
Jul
Aug
Sep
Oct
Nov
Dec
Month

**Figure 6.**

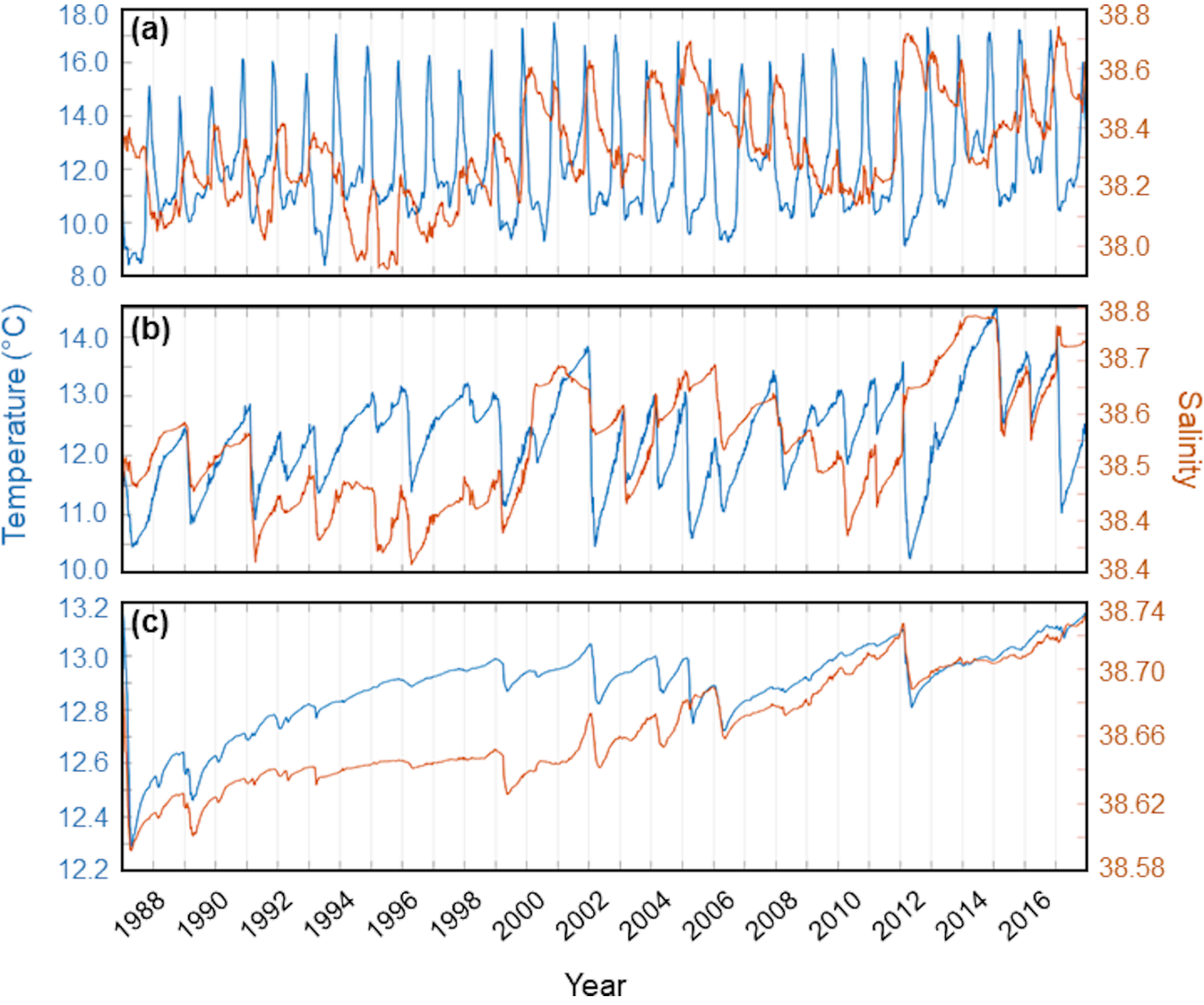
(a)
(b)
(c)
Temperature (°C)
Salinity
Year
18.0
16.0
14.0
12.0
10.0
8.0
38.8
38.6
38.4
38.2
38.0
14.0
13.0
12.0
11.0
10.0
38.8
38.7
38.6
38.5
38.4
38.4
13.2
13.0
12.8
12.6
12.4
12.2
38.74
38.70
38.66
38.62
38.58
1988
1990
1992
1994
1996
1998
2000
2002
2004
2006
2008
2010
2012
2014
2016

**Figure 7.**

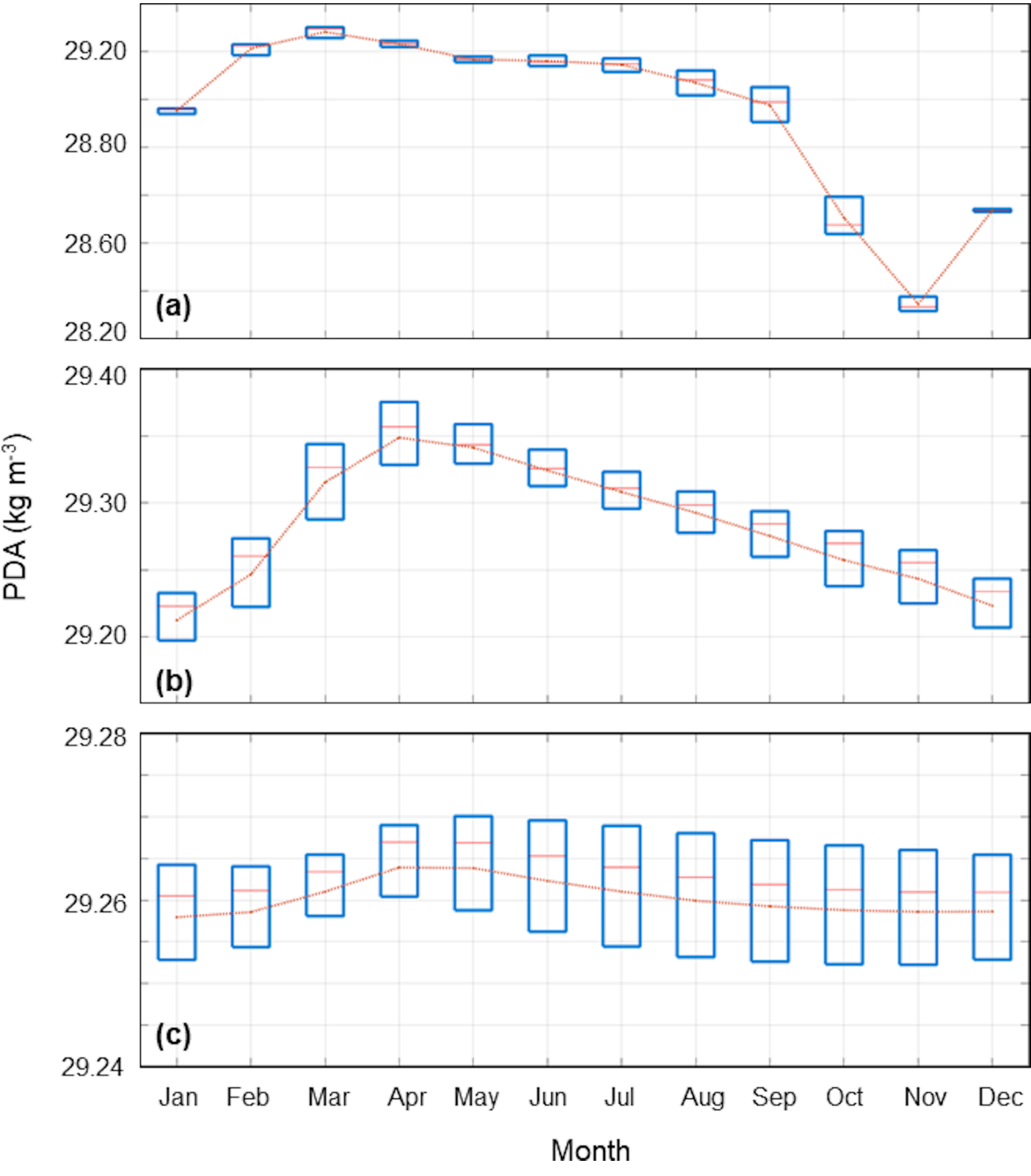
29.20
28.80
28.60
28.20
(a)
29.40
29.30
29.20
(b)
29.28
29.26
29.24
(c)
PDA (kg m-3)
Jan
Feb
Mar
Apr
May
Jun
Jul
Aug
Sep
Oct
Nov
Dec
Month

**Figure 8.**

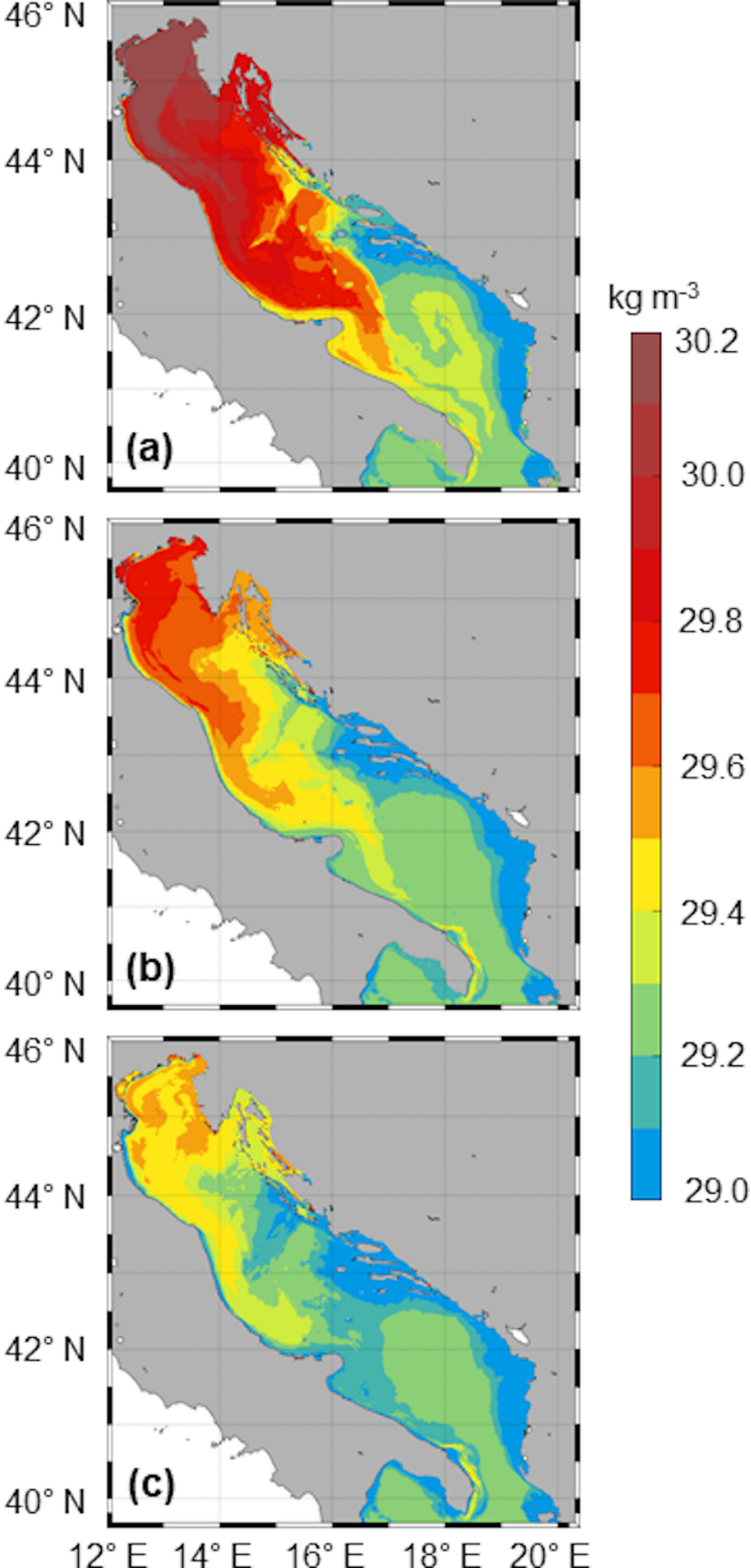
46° N
44° N
42° N
40° N
(a)
(b)
(c)
12° E
14° E
16° E
18° E
20° E
kg m-3
30.2
30.0
29.8
29.6
29.4
29.2
29.0

**Figure S1.**

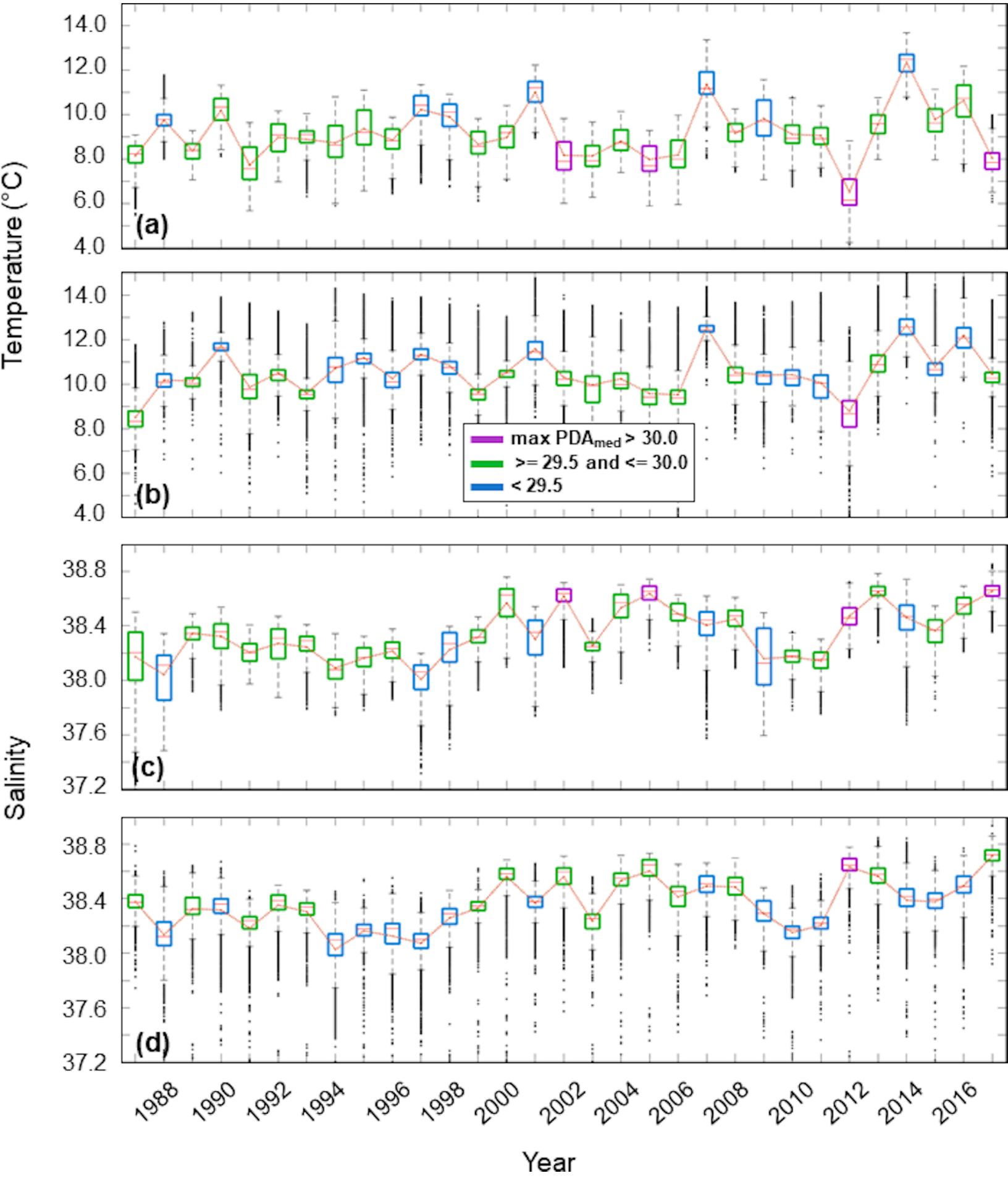
Temperature (°C)
14.0
12.0
10.0
8.0
6.0
4.0
(a)
(b)
max PDA$_{med}$ > 30.0
>= 29.5 and <= 30.0
< 29.5
Salinity
38.8
38.4
38.0
37.6
37.2
(c)
(d)
1988
1990
1992
1994
1996
1998
2000
2002
2004
2006
2008
2010
2012
2014
2016
Year

**Figure S2.**

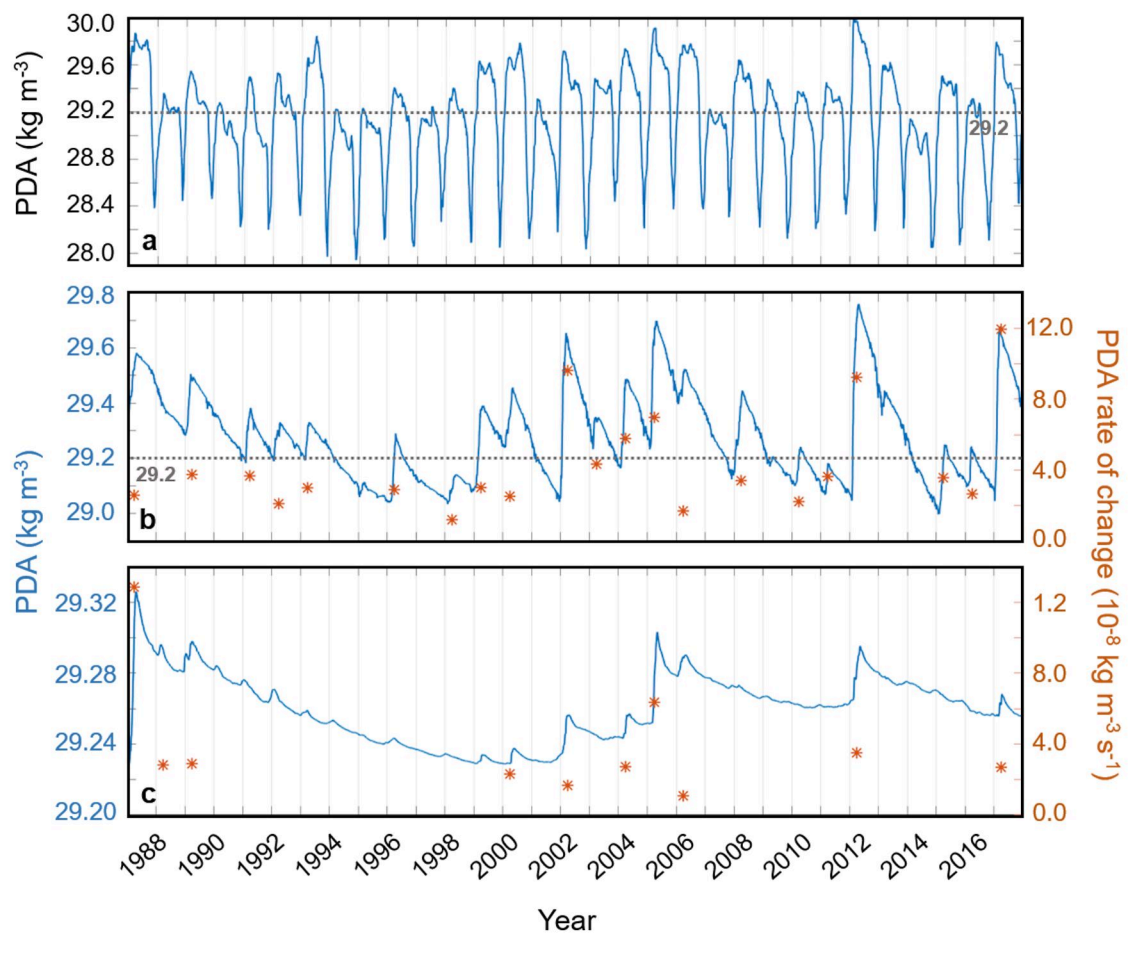
PDA (kg m-3)
30.0
29.6
29.2
28.8
28.4
28.0
a
29.2
29.8
29.6
29.4
29.2
29.0
29.2
b
12.0
8.0
4.0
0.0
PDA rate of change (10-8 kg m-3 s-1)
29.32
29.28
29.24
29.20
c
1.2
8.0
4.0
0.0
1988
1990
1992
1994
1996
1998
2000
2002
2004
2006
2008
2010
2012
2014
2016
Year

**Figure S3.**

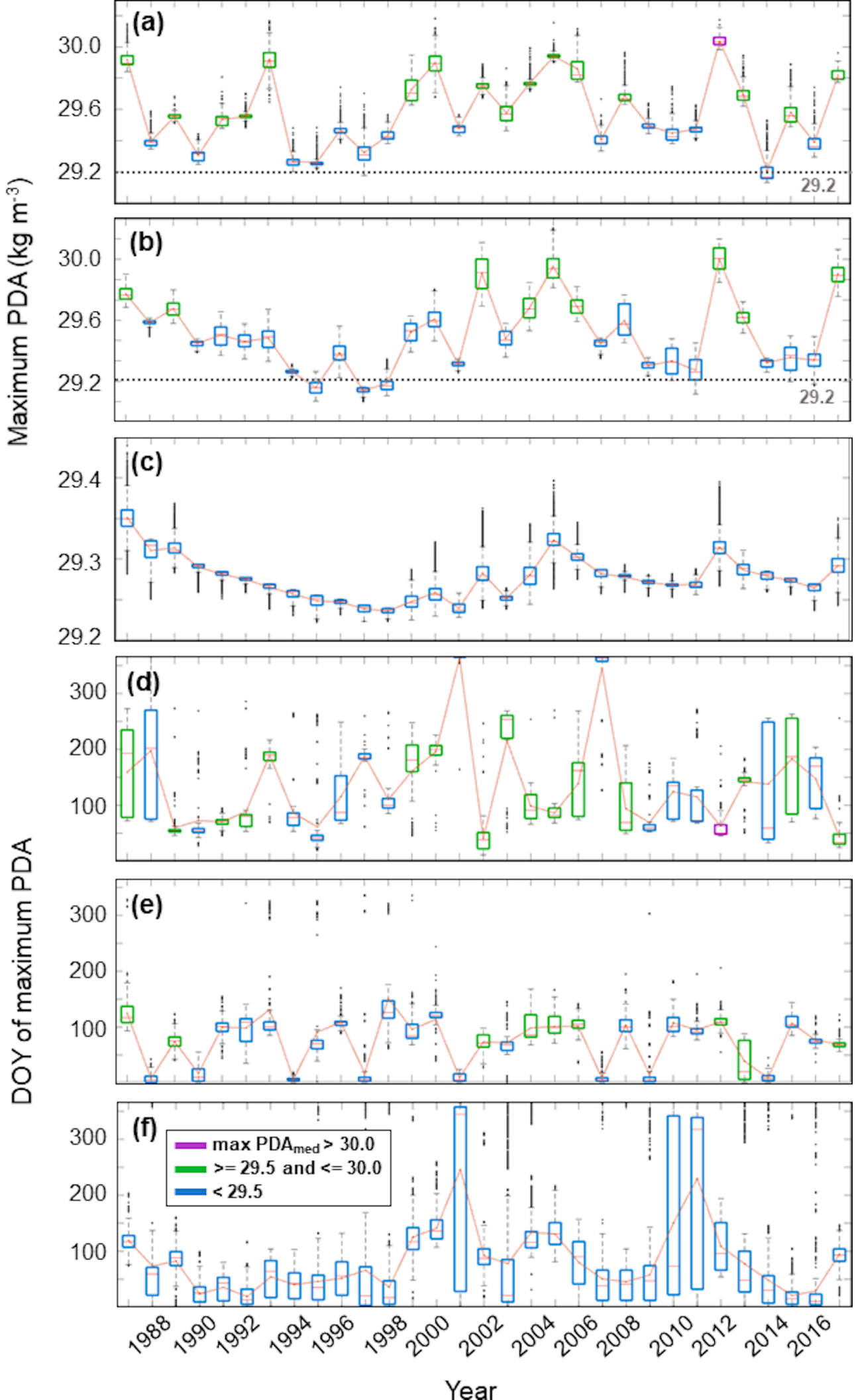
(a)
(b)
(c)
(d)
(e)
(f)
Maximum PDA (kg m-3)
DOY of maximum PDA
30.0
29.6
29.2
29.4
29.3
300
200
100
29.2
max PDAmed > 30.0
>= 29.5 and <= 30.0
< 29.5
1988
1990
1992
1994
1996
1998
2000
2002
2004
2006
2008
2010
2012
2014
2016
Year

**Figure S4.**

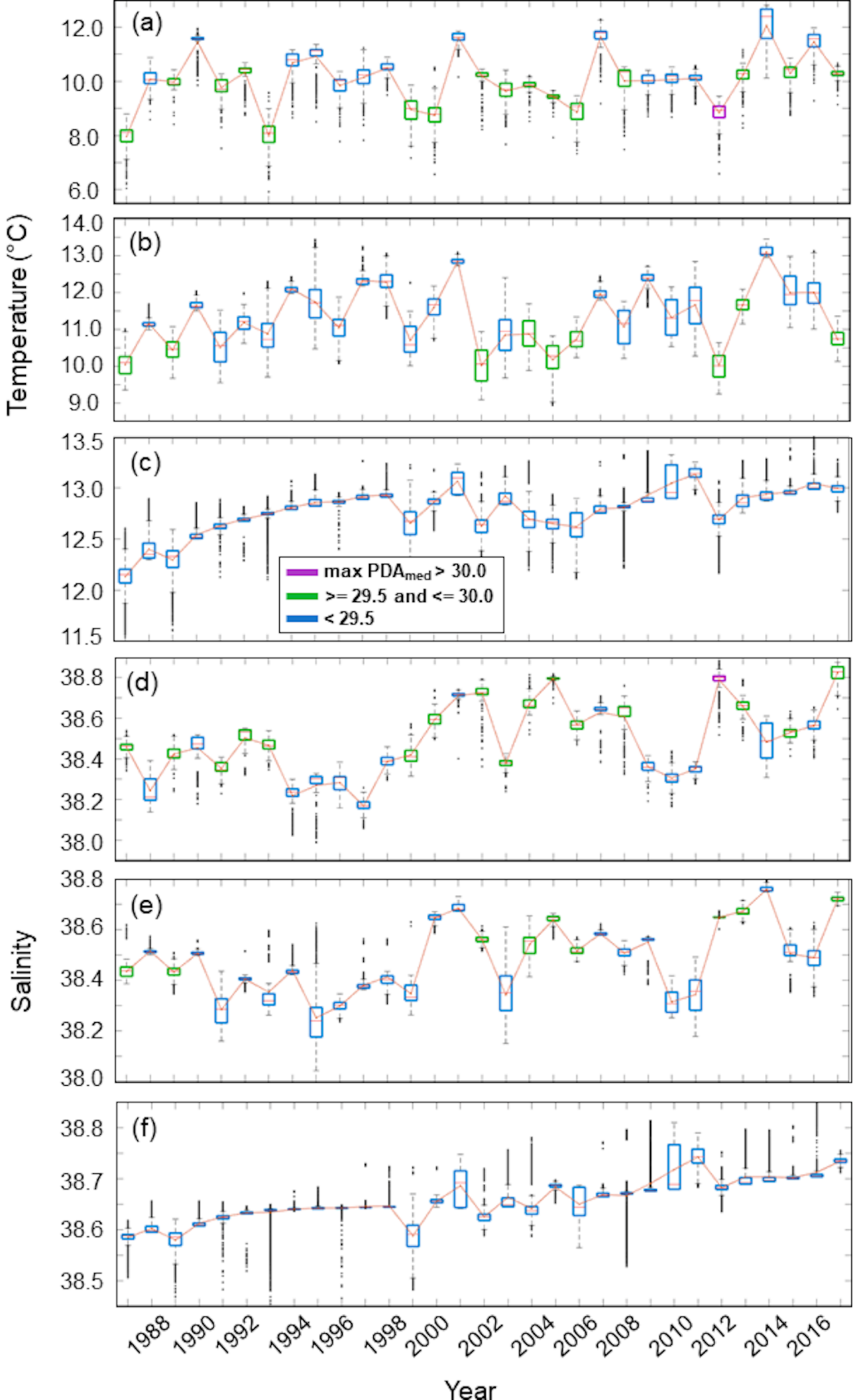
(a)
(b)
(c)
(d)
(e)
(f)
Temperature (°C)
Salinity
Year
max PDA$_{med}$ > 30.0
>= 29.5 and <= 30.0
< 29.5
12.0
10.0
8.0
6.0
14.0
13.0
12.0
11.0
10.0
9.0
13.5
13.0
12.5
12.0
11.5
38.8
38.6
38.4
38.2
38.0
38.8
38.6
38.4
38.2
38.0
38.8
38.7
38.6
38.5
1988
1990
1992
1994
1996
1998
2000
2002
2004
2006
2008
2010
2012
2014
2016

**Figure S5.**

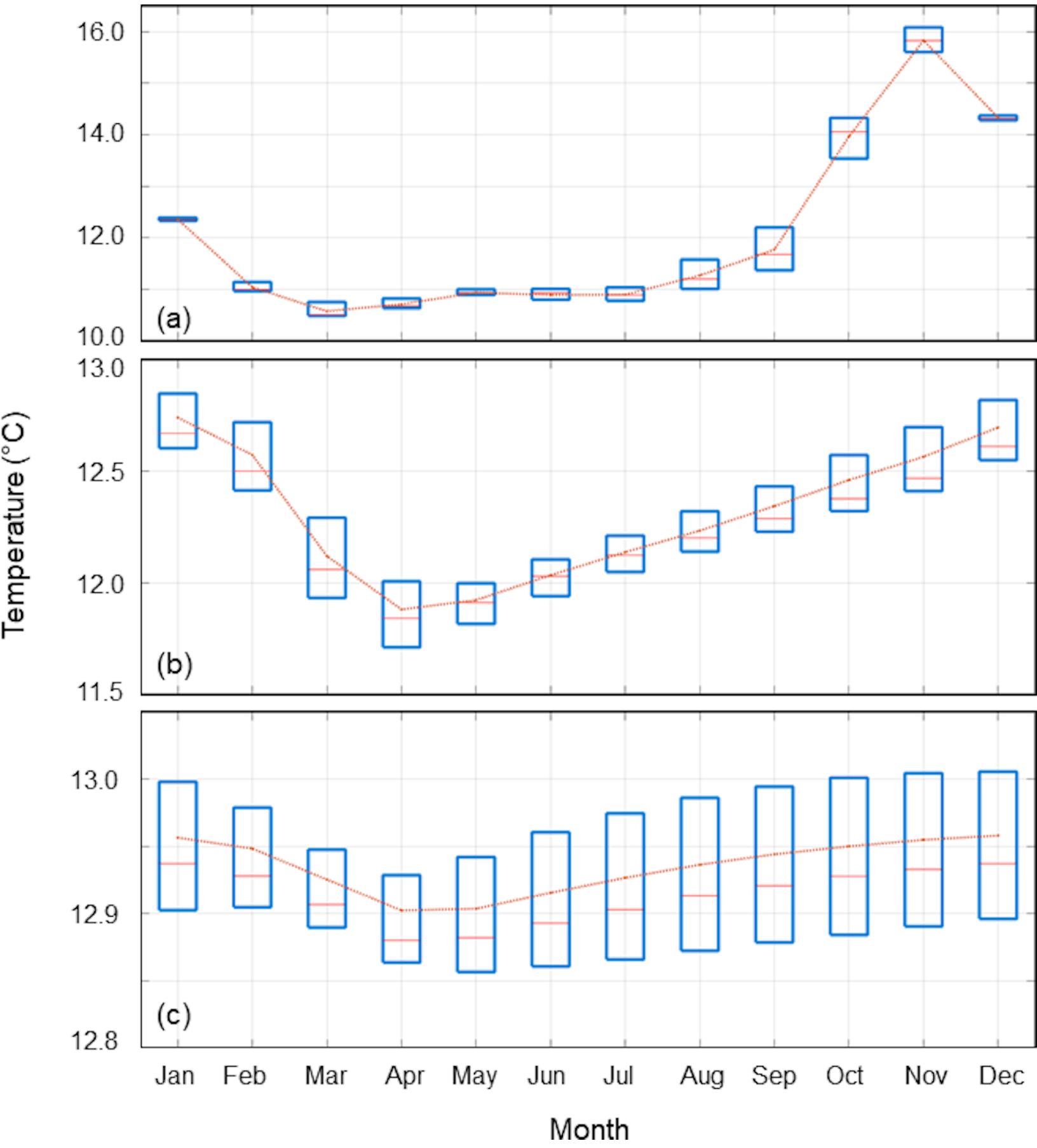
16.0
14.0
12.0
10.0
(a)
13.0
12.5
12.0
11.5
(b)
13.0
12.9
12.8
(c)
Temperature (°C)
Jan
Feb
Mar
Apr
May
Jun
Jul
Aug
Sep
Oct
Nov
Dec
Month

**Figure S6.**

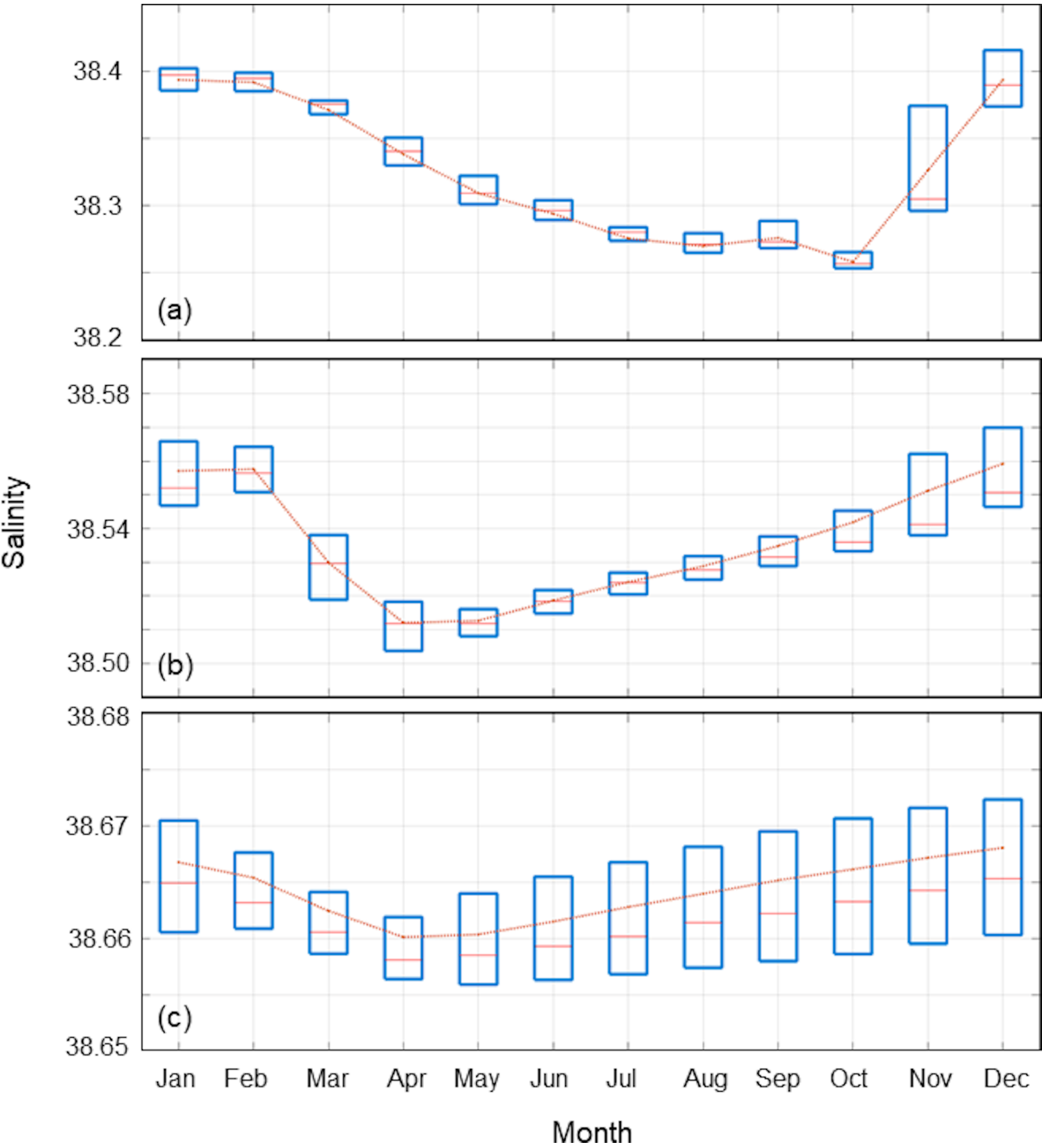
38.4
38.3
38.2
(a)
38.58
38.54
38.50
(b)
38.68
38.67
38.66
38.65
(c)
Salinity
Jan
Feb
Mar
Apr
May
Jun
Jul
Aug
Sep
Oct
Nov
Dec
Month